

MASTER THESIS

Thesis submitted in partial fulfillment of the requirements
for the degree of Master of Science in Engineering at the
University of Applied Sciences Technikum Wien
Degree Program Tissue Engineering and Regenerative
Medicine

The Role of Sideroflexins and Serine Transport in Normal Physiology and Disease

By: Nevena Jankovic, BSc
Student Number: 1710692026

Supervisor 1: Mag. Dr. Elisabeth Simböck
Supervisor 2: Dr. Nora Kory

Vienna, December 14th, 2019



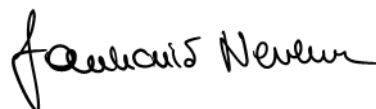
Declaration of Authenticity

“As author and creator of this work to hand, I confirm with my signature knowledge of the relevant copyright regulations governed by higher education acts (see Urheberrechtsgesetz/ Austrian copyright law as amended as well as the Statute on Studies Act Provisions / Examination Regulations of the UAS Technikum Wien as amended).

I hereby declare that I completed the present work independently and that any ideas, whether written by others or by myself, have been fully sourced and referenced. I am aware of any consequences I may face on the part of the degree program director if there should be evidence of missing autonomy and independence or evidence of any intent to fraudulently achieve a pass mark for this work (see Statute on Studies Act Provisions / Examination Regulations of the UAS Technikum Wien as amended).

I further declare that up to this date I have not published the work to hand nor have I presented it to another examination board in the same or similar form. I affirm that the version submitted matches the version in the upload tool.”

Vienna, December 14th, 2019



Place, Date

Signature

Kurzfassung

Der Ein-Kohlenstoff-Metabolismus ist ein kompartimentalisierter Signalweg, bestehend aus einer cytosolischen und einer mitochondrialen Komponente, und wird hauptsächlich von der Serin-Verfügbarkeit gesteuert. Serin ist der Hauptlieferant der Ein-Kohlenstoff-Einheiten und demnach essenziell für die Entwicklung und das Wachstum von physiologisch gesunden Zellen und Krebszellen. Sideroflexin 1 (SFXN1), ein Mitglied der Sideroflexinfamilie, wurde kürzlich als Serin-Transporter in der inneren mitochondrialen Membran und neuer Bestandteil des Ein-Kohlenstoff-Metabolismus' beschrieben. Die Rolle der Sideroflexinfamilie *in vivo* bleibt jedoch unbekannt. Infolgedessen ist es das Ziel dieser Arbeit die Rolle von SFXN1, und die seines redundanten Homologen SFXN3, im gesunden und erkrankten Gewebe zu untersuchen. Um diese Fragen zu beantworten, wurden globale SFXN1 und SFXN3 Knock-Outs mittels CRISPR/Cas9 in C57BL6/J Mäusen generiert und mittels Immunoblotting und Flüssigchromatographie/Massenspektrometrie-basiertem Metabolomics charakterisiert. Menschliche Lymphombiopsien wurden mittels Immunoblotting untersucht, um die Rolle der Sideroflexinfamilie in Tumoren zu verstehen. Die Ergebnisse der *in vivo* Studien zeigen, dass SFXN1 der weitestgehend am Häufigsten exprimierte Homolog der Sideroflexinfamilie ist. SFXN3 wird spezifisch in Geweben des Nervensystems exprimiert. Genotypische und phänotypische Untersuchungen haben eine höhere Neugeborenen Sterblichkeitsrate bei SFXN1 Mäusen gezeigt. Metabolische Untersuchungen zeigen, dass die Deletion eines funktionellen SFXN1 Allels zu metabolischen Veränderungen führt. Auf Grund der Störungen des Ein-Kohlenstoff-Metabolismus werden Zwischenprodukte der Purinsynthese in Leberzellen akkumuliert. Des Weiteren sinkt die Produktion an Harnstoffzyklus' Zwischenprodukten in SFXN1 heterozygoten Mäusen. Der Verlust von SFXN3 führt zu der Herabregulierung von SFXN1 in adulten SFXN3 Knock-Out Gehirnen. Kontrollgewebe wie Leber und Niere sind nicht von solch einer Veränderung betroffen. Die Charakterisierung von menschlichen Tumorbiopsien zeigt eine SFXN1 Überexpression in nicht-weiter-spezifizierten und Diffuses großzelliges B-Zell Lymphomen. Zusammenfassend ist zu sagen, dass die *in vivo* Studien von SFXN1 und SFXN3 Mäusen als auch die Untersuchungen der Lymphombiopsien interessante initiale Trends enthüllen konnten, welche zur Charakterisierung dieser neuen Familie an mitochondrialen Transportern beitragen.

Schlagwörter: Ein-Kohlenstoff-Metabolismus, Mitochondrien, Serin, Sideroflexin, SFXN1, SFXN3, Metabolomics

Abstract

The one-carbon pathway is a compartmentalized metabolic pathway having both a cytosolic and a mitochondrial branch. The pathway is mainly fueled by serine and is essential for survival and proliferation of normal and tumor cells. Sideroflexin 1 (SFXN1), a member of the Sideroflexin family, was recently reported as serine transporter and a novel component of the one-carbon pathway. Yet, its role *in vivo* remains unknown. Consequently, the aim of the presented study is to identify the role of SFXN1, and its redundant homologue SFXN3, in normal physiology and cancer. To analyze the physiology of this transporter, we used C57BL6/J mice with a CRIPSR/Cas9-generated global deletion of SFXN1 and SFXN3, we submitted them to molecular characterization through immunoblotting and liquid chromatography-mass spectrometry-based metabolomics. Human lymphoma samples were used to assess the role of SFXNs in cancer via immunoblotting. In our hands, SFXN1 is revealed as the predominantly expressed member of the SFXN family whereas SFXN3 is specific to the nervous system. Genotypic and phenotypic monitoring of the strains indicates a higher mortality rate in SFXN1 neonates. Loss of one SFXN1 allele leads to alterations of the cellular metabolism leading to an accumulation of purine synthesis and decrease of urea cycle intermediates in the livers of SFXN1 heterozygous animals. The depletion of SFXN3 leads to a decrease of SFXN1 expression in the adult murine brain. Control tissues such as kidney or liver remain unchanged. The analysis of human cancer samples reveals that SFXN1 is likely upregulated in other not further specified (NOS) and diffuse large B-cell (DLBCL) lymphomas. Concluding, the *in vivo* studies of SFXN1 and SFXN3 mice as well as the initial characterization of lymphomas indicate interesting trends shedding light on the functions of an important but poorly understood family of mitochondrial transporters.

Keywords: one-carbon metabolism, mitochondria, serine, Sideroflexin, SFXN1, SFXN3, metabolomics

Acknowledgements

I would like to thank Dr. David Sabatini for granting me the opportunity to write this thesis in this lab.

My gratitude goes particularly to Dr. Nora Kory for accepting me as an intern and allowing me to work with her. Thank you for the talks about science and constructive criticism on the projects as well as the motivating talks about pursuing a career in science. – Thanks for everything!

Additionally, I would like to thank Mag. Dr. Elisabeth Simböck for being my internal supervisor at the FH Technikum Vienna.

I would like to thank all the amazing people who were by my side during this amazing journey! My special gratitude goes here to all the great Master students, Sanne van der Rijt, Daan Overwijn, Pim van der Helm and Anna Platzek in the Sabatini lab as well as Daniel Rotter for the fun times and support. Lastly, I would like to thank my family for all the moral support during my studies.

Table of Contents

1	Introduction	6
1.1	Cell Compartmentalization and Its Contribution Towards Nutrient Management.....	6
1.2	Mitochondria and Metabolism.....	7
1.2.1	Mitochondrial Structure, Organization and Distribution	7
1.2.2	Mitochondrial Role in Cell Metabolism.....	9
1.3	One-Carbon Metabolism	11
1.3.1	The Two Parallel Pathways	11
1.3.2	The Role of Serine in One-Carbon Metabolism	14
1.4	The Sideroflexins.....	15
1.5	One-Carbon Metabolism in Disease	18
1.5.1	One-Carbon and Serine Deficiencies	18
1.5.2	One-Carbon Metabolism, Serine and Cancer	19
1.6	Hypothesis	20
1.7	Project Aim.....	21
2	Materials and Methods.....	22
2.1	<i>Generation of CRISPR/Cas9 SFXN1 and 3 KO mice</i>	<i>22</i>
2.2	Assessment of the Geno- and Phenotype	23
2.2.1	Animal Housing	23
2.2.2	Genotyping Strategy.....	23
2.2.3	Strain Characterization	25
2.3	Western Blotting.....	26
2.3.1	Sample Collection	26
2.3.2	Lysis and Protein Quantification	27
2.3.3	SDS PAGE and Blotting	27
2.3.4	Semi-quantification of SFXN bands	29
2.4	Metabolite profiling using Liquid Chromatography-Mass Spectrometry (LC/MS)...	29
2.4.1	Metabolite Isolation from Murine Tissue Samples.....	29
2.4.2	Sample Preparation and Analysis.....	30
2.5	RNA seq and Graphic Design.....	31

3	Results	32
3.1	Sideroflexin Expression in Humans and Mice.....	32
3.2	Genotypic Characterization of SFXN1 and SFXN3 knockout Mice	35
3.3	Phenotypic Characterization of SFXN1 and SFXN3 KO Mice.....	37
3.4	The Loss of a Functional SFXN1 Allele Leads to a Decrease in SFXN1 Protein Levels and Reveals Changes in the Murine Metabolism	40
3.5	The Loss of SFXN3 Alters SFXN1 Expression in the Brain but not in the Kidney or Liver	44
3.6	Investigating the Role of Sideroflexins in Lymphoma.....	48
4	Discussion	50

1 Introduction

1.1 Cell Compartmentalization and Its Contribution Towards Nutrient Management

A metabolically significant characteristic of the eukaryotic cell is its compartmentalization by membrane-bound organelles. To function properly cells need this subdivision of the intercellular space to allow for efficient metabolite flux facilitating the conversion of substrates and synthesis of new macromolecules required by the organism [1], [2]. Eukaryotic cells are subdivided into the following compartments (in order of relative volume of the cellular space occupied): the cytosol, mitochondria, rough endoplasmic reticulum, smooth endoplasmic reticulum and Golgi apparatus, nucleus, lysosomes, endosomes and peroxisomes [3]. Each of the mentioned compartments contributes to cellular metabolism.

Cellular metabolism is compartmentalized in a spatial and temporal manner [4]. A spatial subdivision of organelles allows the cell to coordinate different metabolic reactions [2], [5]. The different cellular metabolic compartments are not isolated from each other. In contrast, these metabolic hubs are interconnected by metabolic channels [5], [6]. Establishment of metabolic channels offers several benefits for the cell. The controlled flux of the different metabolites and their intermediates retains the waste of energy resources by bypassing unnecessary enzymatic steps [6]. In addition, this metabolic compartmentalization allows for a concentration of enzymes required for the nutrient degradation from microenvironment to microenvironment. This enables the cell to accomplish even energetically unfavorable reactions [7]. Finally, a subdivision of metabolic pathways contributes to an efficient and accurate removal of toxic waste produced by the cell during each one of those intermediate steps [2]. The cytosol, for instance, performs a majority of intermediary metabolism [3]. As an example, the cytosol of the eukaryotic cell is the site of metabolic pathways such as fatty acid biosynthesis and glycolysis. Small molecules are later transported to where they are required for further synthesis steps [8].

Cells are able to modulate their metabolism within a short period of time depending on nutrient availability. Upon metabolite recognition, the activity of enzymes in the corresponding metabolic compartment is changed leading to fine adjustments of post-translational processes. This nutrient sensing allows the cell to adapt in a short period of time. Long-term alterations of the metabolic activity of cells are caused by environmental changes leading to transcriptional alterations in the nuclear compartment and thus adaptation [4], [9].

The coordination of cellular nutrient demands and metabolic compartmentalization highly depends on cell-specific functions of tissues as well as cellular micro- and macroenvironment [1], [4]. Differences in the metabolic requirements of cells determine cell morphology and their exact role in the tissue [10]. For example, cells of the immune system can survive with low nutrient consumption. However, upon cMyc-dependent transcriptional activation, the metabolome of T-lymphocytes switches from a quiescent to an active state resulting in an increased nutrient uptake. This leads to the activation of fatty acid and pyruvate oxidation. The metabolic adaptation consequentially leads to an amplified cell division and growth [11].

1.2 Mitochondria and Metabolism

One organelle in particular is crucial for the maintenance of the cellular metabolism and contributes in this way to cell proliferation and survival. Mitochondria are not only required to produce adenosine triphosphate (ATP) and therefore provide the cell with energy, they are also very important metabolic hubs for both anabolism and catabolism [12], [13].

1.2.1 Mitochondrial Structure, Organization and Distribution

Mitochondria occupy up to one fifth of the cell's total volume and have an approximate outer surface size range from 0.75 to 3 μm^2 [3]. Differences in size result from dynamic changes in mitochondrial morphology caused by fusion and fission [3], [14]. Recent studies have identified that the mitochondrial proteome varies across different tissue types [10]. Furthermore, the number of mitochondria in different tissues vary. As an example, hepatocytes have approximately 5000 mitochondria per cell, whereas adult erythrocytes have none [3].

The mitochondrion is surrounded by two membranes composed of phospholipid bilayers. The membranes differ in size, shape, proteins and lipids localized in the bilayer. The two membranes sub-compartmentalize the mitochondrion into an intermembrane space between the outer and inner membrane and a matrix enclosed by the inner membrane, as shown in **Figure 1** [3].

The outer mitochondrial membrane (OMM) is composed out of different lipids, namely phosphatidylcholine, phosphatidylserine, phosphatidylethanolamine, sphingomyelin and cholesterol [15]. Small molecules and ions, of a size up to 5kDa, can perfuse the outer membrane due to specialized β -barrel-type membrane proteins named porins [3]. Porins connect the aqueous cytosol with the intermembrane space of the mitochondria by forming pores into the 65Å thick OMM [3], [17], [18]. The localization of porins in the lipid bilayer

contributes to a 1:1 phospholipid-to-protein ratio [16]. A schematic depiction of this arrangement is indicated in **Figure 1**.

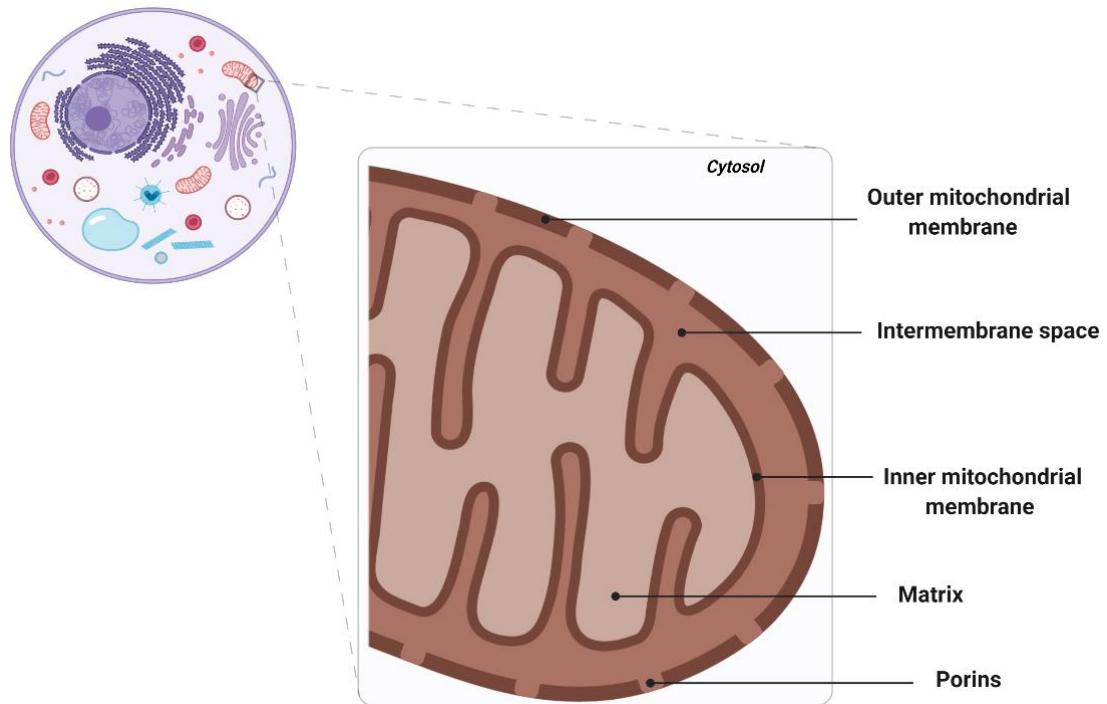


Figure 1: Mitochondria are compartmentalized organelles in eukaryotes. Indicated are schematic depictions of the two limiting membranes (outer and inner) as well as the intermembrane space and the mitochondrial matrix.

The intermembrane space is a narrow gap with an approximate width of 20 to 30 nm located between the outer and the inner mitochondrial membrane [3]. Molecules transported into the intermembrane space need specific receptors or transporters mediating their transportation across the inner membrane and into the mitochondrial matrix [3].

The inner mitochondrial membrane (IMM) surrounds the mitochondrial matrix. This membrane is highly curved, which results in the establishment of cristae. These invaginations of the inner membrane harbor the components of the electron transport chain. By increasing the area of the inner mitochondrial membrane, the cristae also provide a greater surface for oxidative phosphorylation (OXPHOS). OXPHOS contributes to the production of ATP molecules by transferring electrons from donors to acceptors of the respiratory chain. The respiratory chain consists of five key protein complexes, namely complex I (NADH-coenzyme Q oxidoreductase), complex II (succinate-Q oxidoreductase), complex III (Q-cytochrome c oxidoreductase), complex IV (cytochrome c oxidase) and complex V (ATP synthase) [3].

The IMM contains cardiolipin as a component of the phospholipid bilayer. Cardiolipins are required to maintain the membrane potential and stabilize the proteins localized in the inner mitochondrial membrane [16]. Furthermore, a lack of porins in the IMM leads to the establishment of an impermeable boundary. Resulting, the inner membrane requires other classes of transmembrane proteins for the transport of molecules to sustain cellular functions, called solute carriers [18]. Important members of the solute carrier family are the mitochondrial carriers belonging to the SLC25A family, calcium uniporter, pyruvate carrier and Sideroflexins (SFXNs) [19], [20]. All solute carriers have special functions and are differently expressed across tissues types [18]. The IMM has a larger protein to phospholipid ratio than the OMM (3:1), as a result of the different protein complexes harbored in it [3], [16]. By controlling the import and export of molecules across the inner membrane, mitochondria allow the establishment of a viscous compartment, called matrix. The matrix harbors polar metabolites, such as amino acids or nucleotide precursors, as well as the mitochondrial DNA, RNA and protein biosynthesis machinery [3], [18].

1.2.2 Mitochondrial Role in Cell Metabolism

Mitochondria perform complex metabolic tasks for the cell. Their metabolism can be divided into catabolic (respiratory chain), anabolic (fatty acid metabolism, gluconeogenesis, nucleotide synthesis, heme synthesis) and amphibolic (tricarboxylic acid – TCA – cycle) processes [8], [21]. Many metabolite precursors are synthesized in the cytosol of the eukaryotic cell and need to be imported into the mitochondrion to be processed further [18]. Small molecules encounter porins, as the first instance [3]. The intermembrane space contributes toward the connection of the cytosol and the mitochondrial matrix by regulating the exchange of ions, proteins, or other metabolic intermediates [3], [22].

When transported into the mitochondrial matrix, the newly synthesized metabolites can be used for the different metabolic branches within the mitochondria. By contributing to the fatty acid metabolism, these organelles support the maintenances of cell membranes. In addition to the synthesis of phospholipids, mitochondria also play a role in the synthesis of cholesterol by supplying the endoplasmic reticulum with sufficient acetyl-CoA units [3]. The acetyl-CoA units are generated from pyruvate originating from the glycolytic pathway. These units fuel the electron transport chain by supplying coenzymes [3]. The reduction of coenzymes, like FADH₂ (flavin adenine dinucleotide) and NADH (nicotinamide adenine dinucleotide) inside the mitochondrial matrix drives the electron transport chain. These redox reactions lead to the generation of ATP which is used as an energy source [12], [18].

In addition to NADH and FADH₂, the TCA cycle contributes to gluconeogenesis through the synthesis of oxaloacetate [12]. Mitochondrial metabolism additionally supports the detoxification of the cells through the urea cycle. The first and second step of the cycle clear ammonia from the mitochondrial matrix by converting it into citrulline. Citrulline is then

transported into the intermembrane space [18]. This leads to the clearance of excess ammonia, generated through amino acid degradation, by the kidneys [3].

Mitochondria are able to generate amino acids through the process of transamination. Different intermediates of the TCA cycle can contribute to the generation of amino acids. For example, α -ketoglutarate transamination allows for glutamate, proline or arginine synthesis. The transamination of pyruvate leads to the synthesis of serine, glycine and cystine. Oxaloacetate produces amino acids such as methionine, threonine and lysine [23]. The amino acid metabolism allows for the degradation of the metabolites and therefore fuels the synthesis of nucleotides. Depending on the nucleotide required, pyridine or pyrimidine, different amino acid combinations will be required. To produce pyridines, amino acids glutamine, aspartate and glycine are processed. Pyrimidine production, however, calls for amino acids aspartate and glutamate. The nucleotide synthesis requires several single carbon units as well as up to six ATP molecules [3], [8].

The mitochondrial matrix also contributes to the iron metabolism. Iron ions taken up by the mitochondrion are complexed into a porphyrin ring and protoporphyrin IX to form heme. The biosynthesis of heme is initiated inside the mitochondria by a condensation reaction of succinyl CoA and glycine. These metabolites form the heme intermediate 5'-aminolevulinic acid in the mitochondrion. This reaction is performed by aminolaevulinic acid synthase. 5'-aminolevulinic acid is subsequently transported to the cytosol where the synthesis continues until heme is formed [24]. Heme synthesis is as a crucial metabolic pathway, contributing to processes inside and outside the mitochondria. It is a prosthetic group in hemoglobin, myoglobin, cytochromes a and c, catalases and peroxidases. In red blood cells, heme binds and transports oxygen through the organism. Heme is also associated with complexes III and IV as a cofactor. As a shuttle for electrons in the respiratory chain [24], [25].

Furthermore, mitochondria are also involved in redox homeostasis of the cell. Oxidative phosphorylation leads to the generation of reactive oxygen species (ROS) [3]. Metabolites such as ROS are crucial for cellular homeostasis and drive signaling cascades promoting cell growth and survival [26]. In contrast, an excessive production of ROS in the mitochondria leads to the oxidation of macromolecules contributing to the initiation of the programmed cell death, named apoptosis [12]. Apoptosis is a crucial regulator of cell proliferation. There are two different pathways inducing programmed cell death; the intrinsic pathway initiated by intracellular stress and the extrinsic pathway triggered by intercellular stress [3].

Mitochondria respond to the collapse of membrane potential by releasing cytochrome c. This step leads to the activation of pro-apoptotic signals which initiate the release of caspases. Eventually, these caspases will lead to a complex molecular cascade resulting in the permeabilization of the cell membrane [3], [12].

1.3 One-Carbon Metabolism

The one-carbon pathway is a compartmentalized metabolic pathway with a cytosolic and a mitochondrial branch. This metabolic process supplies the eukaryotic cell with single carbon units essential for the development of an organism, the proliferation as well as survival of normal and tumor cells [27], [28].

1.3.1 The Two Parallel Pathways

The one-carbon pathway is mainly fueled by the uptake of single carbon units [29]. Cells have intracellular folate pools located in the mitochondria and the cytosol. Folate is an essential metabolite in mammals and therefore needs to be taken up through the diet. Folate is stored mainly in hepatocytes [30]–[32].

Folates are carriers of one-carbon units and are therefore needed as cofactors of one-carbon metabolism allowing for further metabolic processes [32]. Dietary folates circulate in the organism in their reduced form, namely dihydrofolate (DHF). Folate can enter the cell through two different solute carriers, SLC19A1 and SLC46A1 [33]. SLC19A1 catalyzes the exchange of folic acid for another anion substrate [34]. SLC46A1 functions as a symporter of protons and folates into the cell, as shown in **Figure 2A** [33], [35]. Once folic acid is transported into the cytosol, it is first reduced to DHF. The reduction of DHF to tetrahydrofolate (THF) occurs via the dihydrofolate reductase (DHFR). THF can be later fed into the pathway as an one-carbon donor [32].

One-carbon metabolism consists of two branches, a cytosolic and a mitochondrial, containing isoenzymes which contribute to the parallel cascade of the pathway. The compartments are connected through small molecules required to fuel the metabolism [32], [36]. *In vitro* tracing experiments have shown that the pathway is proceeding, under most conditions, in a unidirectional mitochondrial to cytosolic cycle due to the oxidative environment in mitochondria [37], [38]. Despite mitochondria being the main supplier of one-carbon units, both pathway branches are required to maintain cellular needs through their different functions [38].

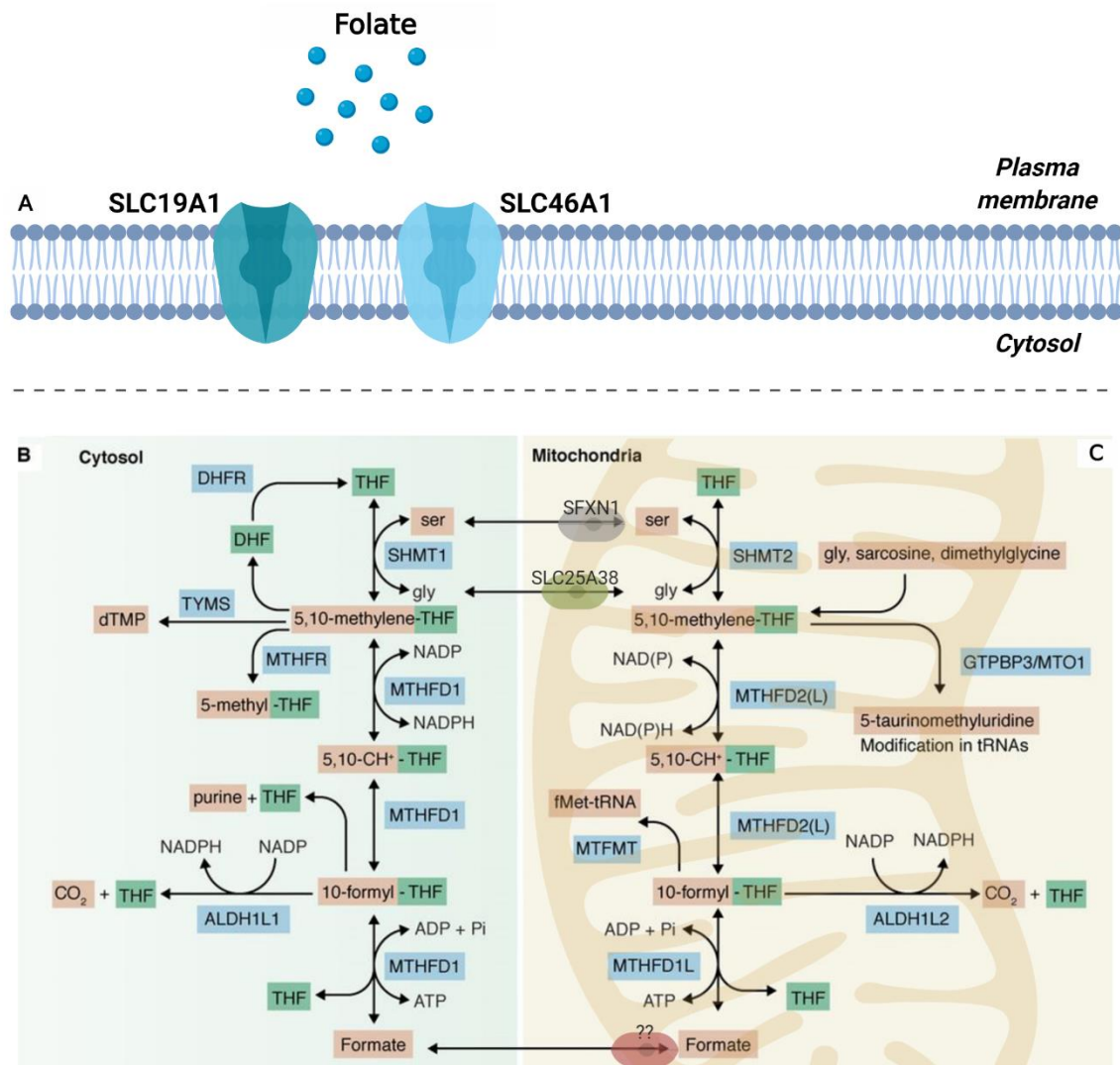


Figure 2: One-carbon metabolism is compartmentalized into a cytosolic and a mitochondrial branch. A: Foliates are transported via solute carrier 19A1 and 46A1 into the cytosol. B: Cytosolic branch of the one-carbon metabolism. Enzymes in the cytosol contribute towards purine and methionine synthesis through one-carbon and formate units from the mitochondrial branch. C: Mitochondrial branch fuels the glycine and formate synthesis. Small molecules can enter the inner mitochondrial membrane through three different transporters; serine via Sideroflexin 1, glycine via SLC25A38 and formate via an unknown transporter. The figure was adapted from Zheng *et al* [33].

The cytosolic branch of the one-carbon metabolism is depicted in **Figure 2B**. Serine hydroxymethyltransferase 1 (SHMT1) transfers carbon units from the non-essential amino acid serine to THF. As a product, THF is reduced to 5,10-methylene-THF and serine is converted to glycine. 5,10-methylene-THF, as well as later on 10-formyl-THF, are presented themselves as important metabolic intermediates. 5,10-methylene-THF is required for three main processes. Firstly, the conversion of 5,10-methylene-THF into deoxythymidine monophosphate (dTMP) by thymidylate synthase (TYMS) leads to the transfer of two

electrons to free THF producing more DHF molecules [36]. Secondly, 5,10-methylene-THF can be reduced to 5-methyl-THF by the methylene tetrahydrofolate reductase (MTHFR). This step leads later to the re-methylation of homocysteine and the forming of methionine [32]. Thirdly, 5,10-methylene-THF contributes to the continuation of the one-carbon metabolism and ultimately leads to the production of free formate units. The cytosolic reduction of 5,10-methylene-THF into 5,10-CH⁺-TF by the 5,10-methylene-THF dehydrogenase 1 (MTHFD1) is NADP⁺ dependent. MTHFD1 also can function as a cyclohydrolase leading to the interconversion of 5,10-methylene-THF via 5,10-CH⁺-TF into 10-formyl-THF. As an intermediate, 5,10-methylene-THF contributes towards *de novo* purine synthesis. Two units of 10-formyl-THF are incorporated into a purine backbone resulting in new nucleotides during purine synthesis [32]. Ultimately, 10-formyl-THF is hydrolyzed by MTHFD1 in an ATP-dependent step into formate. As a result of this reaction, THF is released into the cytosol, which can be either used for the transport of new one-carbon units or be oxidized into CO₂ while generating NADPH for further metabolic steps [36]. The release of formate fuels the production of purines, dTMP and methionine [32], [36].

Figure 2C shows the mitochondrial branch of the one-carbon metabolism. Once transported into mitochondria, serine is cleaved to a reduced form of THF by the serine hydroxymethyltransferase 2 (SHMT2), resulting in the reversible process of glycine production. Consequently, 5,10-methylene-THF is synthesized inside the mitochondrial matrix. Glycine, dimethylglycine and sarcosine contribute towards the formation of mitochondrial 5,10-methylene-THF by donating one-carbon units only to this branch [36]. The mitochondrial branch is able to use synthesized 5,10-methylene-THF to produce 5-taurinomethyluridine. Mitochondria require two different methylene-THF dehydrogenases (MTHFD1 like and MTHFD2 like) for the progression of the pathway; MTHFD2(L) as a dehydrogenase/cyclohydrolase and MTHFD1(L) as a synthetase of formate. MTHFD2(L) is required for the interconversion of 5,10-methylene-THF to 10-formyl-THF. As for the cytosolic branch of the one-carbon metabolism, this conversion is coupled to the intermediate synthesis of 5,10-CH⁺-TF and the reduction of NAD(P) to NAD(P)H [32], [33], [36]. Mitochondrial 10-formyl-THF fate differ in one point from the cytosolic. Instead of contributing to the purine synthesis, 10-formyl-THF can also be processed by the mitochondrial methionyl-tRNA formyltransferase (MTFHMT) as a formyl donor for the initiator methionine-tRNAs. Formylated initiator methionine-tRNAs (fMet-tRNAs) are key factors for the initiation of mitochondrial protein synthesis [39], [40].

The two different branches of the one-carbon metabolism have redundant enzymes involved in the pathway, shown in **Figure 2B** and **C**. This redundancy allows the cells to compensate for the loss of the mitochondrial branch by the cytosolic in case of mitochondrial dysfunction [38].

1.3.2 The Role of Serine in One-Carbon Metabolism

In most organisms, the non-essential amino acid serine is the major one-carbon donor, either directly or through synthesis of other one-carbon donors, such as glycine or formate [41]. The cytosolic serine was shown to be the primary source of one-carbon units for both metabolic branches [36], [42]. Generally, mammals obtain serine from three different sources, as shown in **Figure 3**.

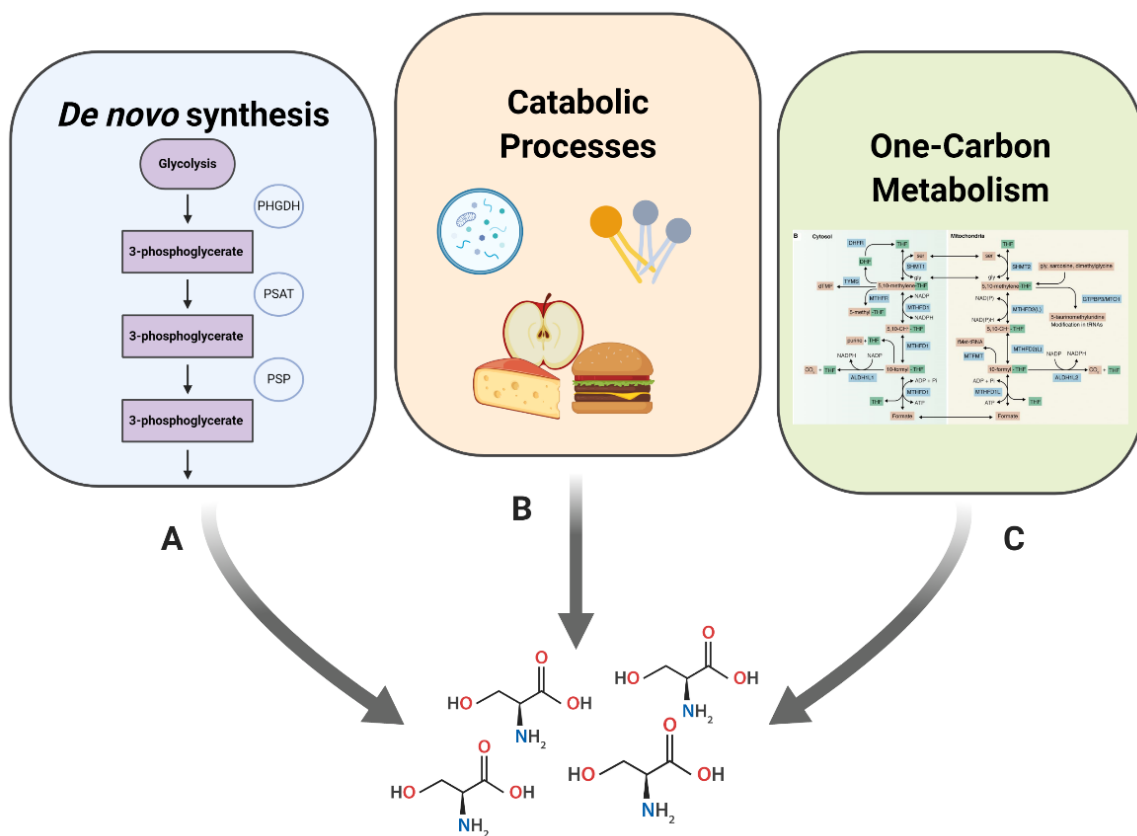


Figure 3: Serine pools are replenished through different pathways. A: Serine *de novo* synthesis. B: Catabolic processes retrieving serine from autophagy, phospholipid metabolism and diet. C: Serine is made via the one-carbon metabolism.

Firstly, serine can be generated through serine biosynthesis in the cytosol. This *de novo* serine synthesis occurs via glycolysis and the serine synthesis pathway. The process requires the activity of three enzymes driving the synthesis of 3-phosphoglycerate to serine. 3-phosphoglycerate derives from glycolysis and is converted by phosphoglycerate dehydrogenase (PHGDH) to 3-phosphohydroxy pyruvate. In the next step 3-phosphoserine is made by the enzyme phosphoserine aminotransferase (PSAT). The final output of the *de novo* synthesis is mediated by the phosphoserine phosphatase (PSP) catalyzing the formation of serine, as depicted in **Figure 3A** [43]. Secondly, serine can be obtained through catabolic processes.

The turnover of phospholipids as well as a dietary uptake of serine contribute to this part of the serine pool, **Figure 3B** [43]. Furthermore, Serine can be taken up through macropinocytosis or autophagy [41], [44], [45]. Thirdly, serine pools can be replenished through the one-carbon metabolism itself. Glycine can be converted to serine by SHMT2 in the mitochondrial branch of the pathway, indicated in **Figure 3C**.

One-carbon units produced from serine catabolism are crucial for the synthesis of intermediates, which are required for DNA and RNA base production, DNA repair as well as for epigenetic maintenance [29], [45], [46]. As described in previous chapters, glycine is a crucial building block for different metabolic processes, as for example purine and heme synthesis [23], [24], [32]. If cells lack an exogenous supply of glycine, they are highly dependent on serine to promote the purine synthesis pathway [32]. Formate, is released into the body and used as a one-carbon donor for purine and thymidylate synthesis across tissues [47]. Further, one-carbon units derived from serine are used to support the methionine cycle and the conversion of methionine to S-adenosylmethionine (SAM). As a cofactor, SAM contributes to DNA and RNA related processes such as histone methylation reactions as well as to the synthesis of the amino acids arginine and lysine [48]. Consequently, modifications of cell signaling pathways, and post-translational alterations can be mediated by the one-carbon metabolism [48], [49].

Besides its crucial role in the production of purines, serine is also involved in the synthesis of amino acids and lipids in cells. The production of cofactors and the assembly of complexes I of the respiratory chain were recently connected to the one-carbon metabolism. An exact mechanism of assembly is still unknown [45], [46], [48], [50], [51]. Furthermore, it is a crucial metabolite required for the synthesis of phosphatidylserine and sphingomyelin [52]. The synthesis of sphingomyelin is especially important for the production of myelin membranes in nervous tissue [43]. Finally, serine-derived one-carbon units are used within the mitochondria to synthesize the reductive equivalents NADH and NADPH and therefore provide the cell-required energy.

1.4 The Sideroflexins

It was established for many years that serine catabolism in mitochondria critically contributes to the one-carbon metabolism; however, the question of how serine enters the mitochondrial matrix remained unanswered.

Kory *et al*/ were able to identify Sideroflexin 1 (SFXN1) as a serine transporter located in the inner mitochondrial membrane in mammalian cells by designing a CRISPR/Cas9-based genetic screen. Based on the current knowledge, the screen was performed in cells lacking serine hydroxymethyltransferase 1 which transfers carbon units from serine to THF [20], [32].

The deletion of SHMT1 results in the loss of the cytosolic conversion of serine to glycine and therefore leads to an impairment of the cytosolic branch of the one-carbon metabolism. The screen revealed SFXN1 as a component of the pathway [20]. SFXN1 was predicted to be a transmembrane protein with five domains conserved in eukaryotic organisms, shown in **Figure 4A** [53]. The deletion of SFXN1 in the follow-up screen performed by Kory *et al* showed metabolic defects in the mitochondrial branch of the one-carbon pathway [20]. Loss of SFXN1 lead to glycine depletion, a reduction in mitochondrial glycine *de novo* synthesis from cytosolic serine and a decrease of glycine amounts in mitochondria when compared to serine. In addition, the purine synthesis intermediates aminoimidazole carboxamide ribonucleotide (AICAR) and glycinamide ribonucleotide (GAR) were accumulated in cells lacking SFXN1 when compared to wild type [20].

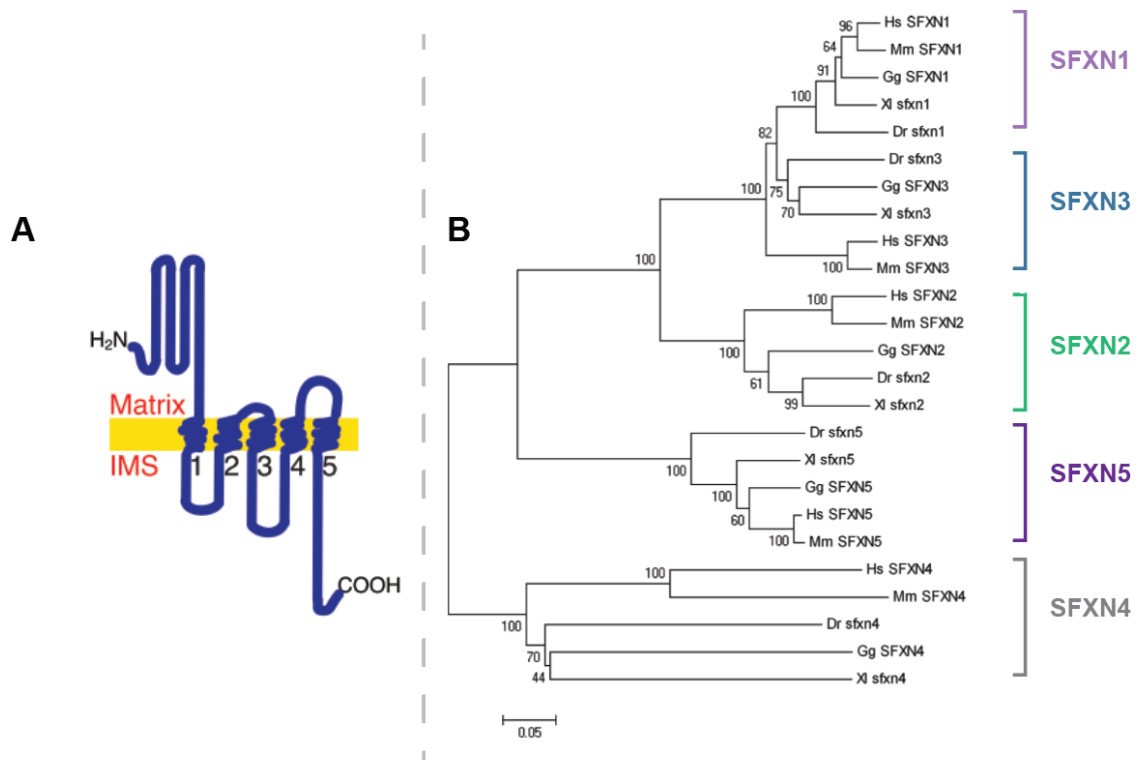


Figure 4: SFXN1 is a transmembrane protein located in mitochondria and expressed across eukaryotic organisms. A: Schematic depiction of SFXN1. SFXN1 has five transmembrane domains (matrix: mitochondrial matrix; IMS: intermembrane space). The figure was adapted from Kory *et al* [20]. B: Homology alignment of the five different SFXNs using ClustalW (Hs: *Homo sapiens*, Mm: *Mus musculus*, Dr: *Danio rerio*, Gg: *Gallus gallus*, Xi: *Xenopus laevis*). Adapted from Li *et al* [54]

Previous sequence analysis showed that Sideroflexins have five homologues in mammals, with SFXN1 and SFXN3 being redundant, **Figure 4B** [20], [55].

Kory *et al* have shown that SFXN3 and SFXN2 are able to rescue the depletion of the mitochondrial glycine pool by transporting serine into the matrix in cells lacking SFXN1. In contrast, SFXN5 is only partially able to compensate the loss whereas SFXN4 is not able to rescue the loss. It is therefore hypothesized that, SFXN4 and SFXN5 might mediate the transport of metabolites other than serine [20].

Originally, the gene *Sfxn1* was identified to be mutated in flexed-tail (f/f) mice. The mice showed two phenotypes, namely anemia and axial changes of the spine [55]. Fleming *et al* described SFXN1 as particularly important during the embryonic hepatic erythropoiesis and therefore the establishment of functional erythrocytes. The study linked the loss of SFXN1 to the observed transient sideroblastic anemia caused by iron accumulation in mitochondria due to the lack of one-carbon units required for heme synthesis [55].

Sideroflexin 3 was described as a mitochondrial protein by Pagliarini *et al* [56]. Rivell *et al* described the detection of SFXN3 in mitochondria localized in the nervous system. In their hands, this protein was expressed higher in neurons when compared to astrocytes [57]. The localization to neurons was also proposed by Simunovic *et al*. The study indicated SFXN3 mRNA levels to be downregulated in the substantia nigra in midbrain dopamine neurons of Parkinson patients [58]. The research conducted by Amorim *et al* identified SFXN3 as a mitochondrial regulator of synaptic morphology. Synapses lacking α -syncline indicated increased SFXN3 protein levels. By overexpressing SFXN3, Amorim and colleagues were able to induce a reduction of synaptic buttons in *Drosophila* neuromuscular junctions resulting in the disruption of synaptic morphology [59]. However, the presented studies were not able to identify the mode of action of SFXN3 in the brain.

SFXN4 was described in a single-patient case study for the first time. This person suffered from macrocytic anemia, which was linked to the loss of SFXN4. However, mechanisms causing the defects remained still unknown [60]. A recent study presented two additional patients lacking SFXN4. Initial experiments indicate that SFXN4 depletion causes severe deficiencies in the respiratory complex I [61]. Sofou *et al* therefore conclude, that SFXN4 is likely to play an important role in the OXPHOS pathway [61]. However, the exact substrate transported by SFXN4 still remains unknown.

SFXN5 was briefly described by Miyake *et al* as a citrate exchanger located to the inner mitochondrial membrane in the brain [62]. No further studies proving or disproving this claim were published so far. The function of SFXN2 was recently published by Mon *et al*. The group revealed that SFXN2 contributes to mitochondrial iron homeostasis by regulating the heme synthesis pathway [63]. Further characterizations of this protein were not presented in the paper. Ultimately, the role of Sideroflexins and their molecular functions besides serine transport are still unclear and require further research.

1.5 One-Carbon Metabolism in Disease

As described, one-carbon units are required for purine synthesis, amino acid and lipid homeostasis, heme synthesis, methylation processes and maintenance of the redox potential [23], [24], [32], [45], [46], [48], [50], [51]. The mammal organism depends on the one-carbon units during developmental processes in the embryonic stage as well as cell maintenance during adulthood [32]. Consequently, dysfunctions of the one-carbon metabolism can result in the development of different malignancies.

1.5.1 One-Carbon and Serine Deficiencies

1.5.1.1 Congenital Sideroblastic Anemia and Heme Synthesis Defects

Tissues with the highest demand in one-carbon units are blood and liver [20]. The one-carbon units delivered to those tissues will mainly be involved in the heme synthesis pathway or processes related to it [32]. If this pathway is impaired, mitochondria will suffer from an iron overload resulting in the manifestation of congenital sideroblastic anemia (CSA). CSA is an inheritable malfunction associated with ineffective erythropoiesis due to an iron accumulation in erythroblasts. The mitochondria of those cells will form a ring around the nucleus presenting the common thread of all CSAs - the ringed sideroblasts. Sideroblasts can be found in the bone marrow of anemia patients. Mitochondria located in these cells are no longer functional [53].

Three main causative changes can be noted. Firstly, sideroblastic anemia can be caused by mutations in genes related to iron or heme metabolism [64]. Fleming *et al* were able to show that the loss of SFXN1 contributes to the formation of sideroblastic anemia [55]. Mutations in other genes contributing to the pathway can lead to different forms of anemias. For example, X-linked sideroblastic anemias are caused by deficiencies of the aminolaevulinic acid synthase 2. Mutations in the glycine transporter lead to the establishment of an autosomal recessive sideroblastic anemia [53]. Secondly, CSA can be caused by perturbations in the iron-sulfur-cluster transport and synthesis [64]. Thirdly, mitochondrial genes can be deleted leading to a defective synthesis of proteins and disruptions of the mitochondrial metabolome [53]. The anemia is most of the time the only manifestation of the disorder. CSA can be detected during different points of a lifetime due to the variation of anemia severity [64].

1.5.1.2 Neurologic Defects and Mitochondrial One-Carbon Metabolism

During embryogenesis one-carbon units are required for the physiological development of the neural tube as well as its further differentiation into the nervous system consisting of the brain and the spinal cord [32]. Studies have presented that the lack of one-carbon units leads to neural tube defects.

More so, the loss of key intermediates and enzymes such as 10-formyl-THF and MTHFD1 in the cytosolic branch of the pathway leads to an embryonically lethal outcome [65], [66]. When deleting MTHFD1L in the mitochondrial branch the same effects on neural development and viability were noted [67].

Serine has been reported to play a role in differentiation, growth and survival of neurons *in vitro*. Moreover, it also contributes to a physiological synaptogenesis and the development of dendrites [68]. Resulting, defects in serine synthesis will cause similar defects in the neurological development. A deficiency in serine *de novo* synthesis leads to a dramatic decrease in serine levels. Due to the impaired serine synthesis, the organism relies on serine uptake through diet. However, cells are not able to generate the same amounts of serine through diet as they would through the intracellular mechanisms; therefore, resulting in a lack of one-carbon units deriving from the SHMT2-mediated serine to glycine conversion. Consequently, severe neurological and growth defects can be noted thus explaining the effects seen with 5,10-methylene-THF dehydrogenase 1 (MTHFD1) and methylene-THF dehydrogenases 1 like (MTHFD1L) deletions resulting in an impaired synthesis of formate in either the cytosolic or mitochondrial branch of the one-carbon pathway [30], [43].

1.5.2 One-Carbon Metabolism, Serine and Cancer

Both increased serine *de novo* synthesis rates and an increased production of one-carbon units have been shown to contribute to tumor development [69]. The overexpression of serine synthesis and catabolic enzymes is promoted by oncogenes such as cMyc. Therefore, tumor cells expressing amplified levels of cMyc are highly dependent on serine to be able to survive under hypoxic conditions and limited nutrient supply as well as produce the building blocks necessary for rapid proliferation [70].

PHGDH is the rate-limiting enzyme in serine biosynthesis. And PHGDH amplifications therefore influence the serine synthesis [32]. However, not only the serine biosynthesis is affected by malignant transformation of the cellular metabolism. Recent studies have revealed an overexpression of enzymes linked to the mitochondrial compartment of the one-carbon metabolism in tumors [50], [71]. This is only possible due to cMyc's role as a controller for both pathways [70]. Changes of the folate metabolism are caused by the upregulation in MTHFD2 and SHMT2 in human cancer cell lines and cancer samples [71], [72]. These upregulations were mainly linked to aggressive cancer types such as melanomas, hepatomas and breast cancer [32], [71]. In addition to the amplification of the mitochondrial one-carbon synthesis, cancer cells also cause changes in the cytosolic compartment of this pathway. Malignant cells require a higher turnover of purines and pyrimidines which results in overexpression of the enzyme thymidylate synthase [32].

Since SHMT2 was shown to be upregulated in cancer samples, Kory *et al* hypothesized that SFXN1 is likely upregulated as well. *In silico* experiments have predicted the highest SFXN1 mRNA levels in blood cancers. The results correlate with the fact that SFXN1 is highly expressed in the hematopoietic lineage [20].

Lymphomas belong to a sub type of blood cancers developing from transformed blood cells [73]. They can be divided into two major categories: Hodgkin (HL), caused by lymphocytes, and non-Hodgkin lymphomas (NHL), caused by different immune cells. 90% of all detected lymphomas are non-Hodgkin lymphomas [74]. The different forms of NHL were classified by the World Health Organization into two major groups. First, mature B-cell neoplasms, resulting from clonal neoplasms of mature B-cells circulating in the bone marrow and the blood [75]. As for example, chronic lymphocytic leukemia (CLL), mantle cell lymphoma (MCL), diffuse large B-cell lymphoma (DLBCL) and other not further specified (NOS) lymphomas [75], [76]. Second, mature T- and NK-neoplasms, resulting from clonal neoplasms of mature T- and NK-cells circulating in the bone marrow [75].

The formation of lymphomas is mainly mediated through changes in the patient's immune system. Both, HL and NHLs can be caused by an infection with the Epstein–Barr virus. Furthermore, HL requires a genetic pre-disposition. NHLs can be also caused by autoimmune diseases [73], [77]. According to the American National Cancer Institute (NCI), 4.2% of all detected cancer cases in the US are NHLs by affecting 23.9% of the male and 16.2% of the female population. NCI recorded 74 200 new cases of NHL and is estimating that 19 970 patients may succumb to this disease [73]. The standard, first-line treatment is the anti-folate methotrexate, which blocks one carbon metabolism by inhibiting the synthesis of THF and therefore the DNA and RNA synthesis [48].

1.6 Hypothesis

SFXN1 was recently reported to be a serine transporter in the inner mitochondrial membrane and novel component of the one-carbon pathway. Current RNA sequencing data sets suggest that Sideroflexins are broadly expressed across tissues with SFXN1 being the predominantly expressed homologue across different tissue types [20].

To answer the question of what roles SFXN1 plays *in vivo*, we propose to study mice with a global deletion of SFXN1. Because SFXN1 has a homologue with overlapping function, namely SFXN3, we will also study SFXN3-null mice. These studies should provide us with an initial insight on the physiological role of SFXNs.

SFXN1 is likely a target of the oncogenic transcription factor cMyc [20]. We hypothesize that due to its function in providing the cell with essential building blocks, such as one-carbon units and glycine, used for nucleotide synthesis, SFXN1 may play a role in tumor maintenance and survival. The dependency of tumors on serine and one-carbon units may support this hypothesis [70].

1.7 Project Aim

The global aim of this thesis is to understand the role and importance of Sideroflexins in normal physiology and in disease. Two aims are presented.

The expression of the protein in different tissues requires verification. Moreover, a characterization of their function *in vivo* may provide insight into tissue-specific functions of these poorly understood mitochondrial transporters and reveal additional functions besides serine transport. To be able to do this, we aim to establish constitutive SFXN1 and SFXN3 knockout (KO) mice by using the clustered regularly interspaced short palindromic repeats (CRISPR)/Cas9 system.

To assess the role of the different SFXNs in malignancies, we will focus on their role in blood cancer. Here, we aim to determine if the serine transporter and its homologues are upregulated in cancer samples as might be expected based on previous studies implicating one-carbon metabolism in this disease. To this end, we will determine Sideroflexin protein levels in normal and cancer tissue. For the analysis, samples from lymphoma patients will be supplied by a clinical collaborator.

2 Materials and Methods

2.1 Generation of CRISPR/Cas9 SFXN1 and 3 KO mice

The animal experiments were designed in compliance with the U.S. Animal Welfare Act and Public Health Service Policy. Experiments were conducted in accordance with the submitted protocols. Used protocols were approved by the Whitehead Institute Committee on Animal Care.

For the characterization of SFXN1 and 3, constitutive CRISPR/Cas9 SFXN1 and 3 KO mice were created. The animals were generated with the help of the Genetically Engineered Models (GEM) Core Facility at the Whitehead Institute following a protocol established by Yang *et al* [78].

Several small guide RNAs (sgRNAs) were designed targeting the two different genes. A list of the used guides and their corresponding target sites are listed in **Table 1**. All guides were cloned into a pX330 plasmid containing a Cas9 coding region. The sgRNA was expressed, purified and stored until use.

Table 1: Small guide RNAs designed to target SFXN1 and SFXN3

<i>Gene of interest</i>	<i>Exon</i>	<i>Guide Number</i>	<i>sgRNA Sequence with PAM Site</i>
<i>Sfxn1</i>	3	sgRNA#1-1_3	TAGCTCATTTCCTGAGGC CGG
<i>Sfxn1</i>	8	sgRNA#1-2_8	AGGTGTTTCATGATAACGGA GGG
<i>Sfxn1</i>	5	sgRNA#1-1_5	GGCCGTTGCCACAGCGCCAG TGG
<i>Sfxn1</i>	9	sgRNA#1-1_9	GGATTGGCGCACTCATCCAC GGG
<i>Sfxn3</i>	3	sgRNA#3-1_3	AGCATTCCATCCGGACACGG GGG
<i>Sfxn3</i>	5	sgRNA#3-1_5	CCCAGTGGTGGCACTCACAT AGG
<i>Sfxn3</i>	6	sgRNA#3-1_6	ACGAATCGACCGACTAGCGG GGG
<i>Sfxn3</i>	7	sgRNA#3-1_7	CAGGTGGTGATATCAAGAAT CGG

In parallel, 12 female 4 weeks old C57BL6/J mice were injected with pregnant mare serum gonadotropin (PMSG). The animals were injected with human chorionic gonadotropin (hCG) after 3 days and housed with male mice overnight. Only females with formed plugs were collected for zygote isolation on the next morning. The animals were euthanized, zygotes were collected from the oviduct and placed in warm potassium simplex optimization medium (KSOM). Zygotes were cultured at 37°C, 5%CO₂ while the guide/Cas9 mixture was prepared

for the injection. The zygotes were placed in Cytochalasin B containing M2 handling media 30 minutes before injection. The first cohort of embryos was injected with all SFXN1 and SFXN3 guides. The blastocysts were genotyped and the guides with the best efficiency were chosen. A second cohort of zygotes was collected as described above. 23 zygotes were injected with SFXN1 sgRNA#2, targeting exon 8, and SFXN3 sgRNA#1, targeting exon 5. Upon injection, all zygotes were placed in KSO media and cultured at 37°C, 5%CO₂ until the blastocyst stage was reached. Blastocysts containing the knockout guides were transferred into the uteri of surrogate mothers. The homozygous SFXN1 and 3 KO mice were back crossed to wild type C57BL6/J mice to start generating pure KO strains.

2.2 Assessment of the Geno- and Phenotype

2.2.1 Animal Housing

Standard housing and cage bedding were provided for all mice as well as burying and nesting material. The animals were fed *ad libitum* with standard irradiated PicoLab chow (Irradiated Rodent Feed; #5053). Breeding cages were weaned 21 days post pup birth and separated by sex. The mice were tagged using numbered aluminum clips. Tagging punches were collected in 1.5ml microcentrifuge tubes for the genotyping procedures.

2.2.2 Genotyping Strategy

To assess the genotype of born mice, DNA was extracted from the collected DNA punches. 50µl of the Quick Extract DNA extraction solution (Lucigen; #QE09050) was added to the tissues and vortexed for 20 seconds. Next, the samples were boiled at 65°C for 6 minutes. Subsequently, tissues were vortexed for 10 seconds and boiled for further 2 minutes at 98°C.

The genotyping of the SFXN1 and 3 strains occurred using a polymerase chain reaction (PCR) based approach. For the initial genotyping of the alleles resulting from CRISPR/Cas9 gene-editing, primers were designed creating a 439 base pair long amplicon for murine SFXN1 (NC_000079.6; NCBI) and a 396 base pair long amplicon for murine SFXN3 (NC_000085.6; NCBI).

To detect the changes in the two respective genes, primers were designed flanking the sgRNA cutting site in both genes. The amplicons were designed to be in the middle of the sequence. The primer sequences are presented in **Table 2**. The master mix was made using the Q5 polymerase kit (New England Biolabs; # M0491L) supplemented with 10µM dNTPs and the corresponding primer. An Eppendorf master cycler X50i/S with the temperature profile shown in **Table 3** was used.

Table 2: Sequences of PCR primers made for both genotyping approaches**Next Generation Sequencing**

Gene	F: Forward Primer R: Reverse Primer	Amplicon Size
<i>Sfxn1</i>	F: TGCAGATTTAAGTGGCTCTGTCT R: CACAGGCACTCACAGTCACT	399 base pairs
<i>Sfxn3</i>	F: CGAGTTCTGTTACCTCCCC R: TGAGAGGGCATCAAGGAGGA	396 base pairs

Regular PCR Genotyping Primers

Gene	F: Forward Primer R: Reverse Primer	Amplicon Size
<i>Sfxn1</i>	F: AGCCATCCCTCCGTTT R: CACAGGCACTCACAGTCACT	369 base pairs
<i>Sfxn3</i>	F: CGAGTTCTGTTACCTCCCC R: GTGGCACTCACATAGGCTGTC	278 base pairs

Table 3: Temperature Profile for both NGS Sequencing PCRs

Stage 1	Stage 2			Stage 3	Hold
98°C	98°C	59°C	72°C	72°C	4°C
30sec	10sec	15sec	35sec	2min	∞
		30			

A 1% agarose gel (Invitrogen; #16500-500) was prepared and stained using 10µg/ml ethidium bromide (Sigma; #E1510-10ML). 3µl of a 1kb DNA standard (New England Biolabs; #N0550S), 5µl of each sample and 5µl of an internal negative control were loaded and ran for 30 minutes at 130V. The amplifications of the desired amplicons were confirmed using the c600 Azure imager. The PCR products were purified using the QIAquick PCR purification kit (Qiagen; #28106) according to the manufacturer's manual. DNA concentration was measured using a NanoDrop spectrophotometer, diluted to a final concentration of 40ng/µl and submitted to next generation sequencing by the MGH genomics core.

Upon the characterization of the deletions, specific PCR primers were designed. The forward primer of SFXN1 was made with a starting point in the deleted region. For SFXN3 a reverse primer was made starting in the altered region of the exon. Depending on the SFXN3 genotype an amplicon size of 278 base pairs (wild type allele), 251 base pairs (heterozygous allele) or no amplification (KO) will be synthesized. The same genotyping strategy was also designed for SFXN1.

The temperature profile was optimized for the different primer pairs, see **Table 4** and **Table 5**. The sequences of the different primers are noted in **Table 2**. A pre-made GoTaq Mastermix (Promega; #M7123) was supplemented with primers, DNA template and using an Eppendorf master cycler X50i/S. To visualize the band shift between heterozygous and wild type animals, products were loaded on a 4% agarose gel and ran as described above.

Table 4: Temperature Profile for the SFXN1 genotyping PCR

Stage 1	Stage 2			Stage 3	Hold
95°C	95°C	55°C	72°C	72°C	4°C
2min	45sec	45sec	45sec	5min	∞
	30				

Table 5: Temperature Profile for the SFXN3 genotyping PCR

Stage 1	Stage 2			Stage 3	Hold
95°C	95°C	56°C	72°C	72°C	4°C
2min	45sec	45sec	45sec	5min	∞
	30				

Due to the fact, that only 8 base pairs are deleted in the SFXN1 KO mice, the genotyping of this strain was outsourced to Transnetyx (Cordova, TN). Transnetyx designed a qPCR-based assay to determine the genotype of the SFXN1 mice. 3mm ear punches were collected and sent to the company for testing.

2.2.3 Strain Characterization

For the basic phenotypic characterization of the SFXN1 and 3 mice, the numbers of all litters and pups per breeding were noted to be able to estimate the reproductive capacity of both strains. The statistical analysis of the litters occurred using GraphPad Prism 8.0. Data normality was assessed by the D'Agostino & Pearson test as well as the Shapiro-Wilk test. Unpaired two-tailed t-tests (parametric, t test with Welch's correction or non-parametric, Mann-Whitney test) were applied and the p-value was set to 0.05. Error bars in the graphs indicate the standard deviation.

In addition, pups were visually monitored for the transient anemia linked to the predicted phenotype. After weaning, SFXN1, SFXN3 and wild type mice were weighed every week over the course of 6 weeks. Both sexes and the three different genotyped were age-matched litters. A total of five animals per sex/genotype were weighed. Furthermore, glucose levels of the two new established strains were compared to the wild type. In addition, the impact of fasting on the different strains was analyzed. Mice were weighed 26 hours before and after

an 18 hour fasting period. To be able to collect blood for the glucose measurement, mice were fixed using an acrylic small diameter restraint. A small incision was made in the tail tips and the flowing blood was used for the glucose measurement (Free Style Freedom Lite). The statistical analysis of body mass and glucose levels occurred using GraphPad Prism 8.0. Kruskal-Wallis test with Dunn's multiple comparisons test was used to analyze the loss of body mass. A one-way ANOVA test with Tukey's multiple comparisons test was used to analyze the glucose levels. The p-value was set to 0.05. Error bars in the graphs indicate the standard deviation.

2.3 Western Blotting

2.3.1 Sample Collection

To address the role and determine the expression of SFXNs *in vivo* wild-type C57BL6/J mice were used to elucidate the expression profile of the five homologues in different tissues. For this experiment one male and one female 7 week old mouse was used. The mice were housed as described above and fed *ad libitum*. Mice were weighed and euthanized by cervical dislocation. Following tissues were collected from both animals: liver, kidneys, adrenal glands, pancreas, spleen, brown fat tissue, heart, lungs and thymus. As a skeletal muscle sample, *Musculus gastrocnemius*, a member of the calf muscle group, was isolated. Next, components of the nervous system, spinal cord, cortex and cerebellum, were obtained. Lastly, the female and the male reproductive system, ovaries for the female and testis for the male animal, were isolated. The livers and brains were weighed, and the values were noted down.

For the comparison between heterozygous SFXN1 and wild type protein expression, two female mice at an age of 7 weeks were used. The mice were weighed, euthanized by cervical dislocation and cortex, cerebellum, liver, kidney, spleen and brown fat samples were collected. The liver and the brain weight were noted down.

All tissue samples for metabolite profiling of the heterozygous SFXN1 and SFXN3 KO animals were collected and processed in the same manner.

The human samples were obtained through a medical collaboration at the Massachusetts General Hospital, Boston, MA. Tissue biopsies of DLBC lymphoma, NOS lymphoma and tonsils from different patients were collected and weighted. 40-50mg per sample were used for the lysis whereas the remaining punches were stored at -80°C.

In all cases, tissues for direct lysis were stored on ice in pre-labeled 1.5 ml microcentrifuge tubes (Axygen®/Corning; #MCT-150-C). Remaining samples were transferred to 2ml cryogenic vials (Corning; #430488), snap-frozen in liquid nitrogen and stored at -80°C.

2.3.2 Lysis and Protein Quantification

The following steps were performed on ice. Samples used for the protein isolation were cut into small pieces to allow for a more rapid cell disruption. RIPA lysis buffer (150mM sodium chloride, 1% Triton X-100, 0.5% sodium deoxycholate, 0.1% sodium dodecyl sulfate - SDS, 50mM Tris + phosphatase and protease inhibitors) was added to the tissues. The volume was adjusted according to the tissue size. Samples and buffer were transferred into a glass douncer and homogenized using an aluminum pestle. The homogenate was poured back into the 1.5ml microcentrifuge tubes. All samples were moved to a rocker at 4°C for 15 minutes. After the incubation step, samples were centrifuged at 21130 x g (maximum speed) for 15 minutes at 4 °C using a benchtop microcentrifuge (Eppendorf, # 10755822). The supernatant was removed and collected in a new tube.

A Pierce bicinchoninic acid assay (BCA assay; Thermo Scientific, #1850978) was used to determine the protein concentration of the lysates. For the standard curve, a stock solution of 2mg bovine serum albumin (BSA; Sigma Aldrich, # A9418-500G) was diluted in 1ml Milli-Q® water. A geometric dilution was prepared from the stock (1mg/ml, 750µg/ml, 500µg/ml, 250µg/ml, 125µg/ml, 62.5µg/ml). The tissue samples were diluted using Milli-Q® water. The Pierce BCA solution was prepared, consisting of a 50:1 dilution of Reagent A to Reagent B. 5µl of each standard, a water sample (blank) and the tissue dilutions were pipetted in triplicates into a 96-well-plate. 200µl of the prepared Pierce BCA solution were added to all wells using a multichannel pipette. The plate was incubated at 37°C for 30 minutes and read afterwards using the SpectraMax iD5 plate reader (Molecular Devices) set at 562nm.

2.3.3 SDS PAGE and Blotting

All murine samples were prepared at a concentration of 40ng protein per 10µl for immunoblotting. The human samples were concentrated at 50ng protein per 10µl. For a total volume of 150µl, 600ng of protein were diluted with RIPA lysis buffer to a volume of 120µl. 30µl of a 5X sample buffer (10% SDS, 3.575M β-mercaptoethanol, 25% glycerol, 308mM Tris-HCl pH 6.8, 830µM bromophenol blue) were added. The samples were boiled at 55°C for 5 minutes. Both the native protein lysates and the prepared immunoblotting samples were stored at -20°C.

Pre-casted 4-20% Novex™ Tris-Glycine midi (Invitrogen; #1908733) and 12% Novex™ Wedged Well Tris-Glycine mini gels were used. The gels were mounted into the

corresponding cells and 1X SDS (25 mM Tris, 192 mM glycine, 0.1% SDS) running buffer was added. 9µl of the protein standard (Color Protein Standard – New England Biolabs; P7719S) and 10µl of each sample were loaded onto the gels. The gels ran at constant voltage; 100V for 3 hours for the midi and 2 hours at 120V for the mini gels. 0.45µm polyvinylidene fluoride membranes (Merck Millipore; IPVH00010) were activated in pure ethanol for 15 seconds, rinsed with de-ionized water and stored until the run was complete. The gels were removed from the cast and rinsed using de-ionized water. Membranes and gels were stacked between Whatman filter papers (GE Healthcare; #303-017) and submerged in transfer buffer (8.8g 3-(Cyclohexylamino)-1-propanesulfonic acid, 13 tablets sodium hydroxide, 400 ml 96% ethanol, 3600 ml di-ionized water).

Protein was transferred at 40V for 2 hours. After the transfer was completed, membranes were blocked in 5% milk/tris buffered saline with tween (TBS-T; 20 ml 1M Tris-HCl pH 7.5, 3,3 ml 5M NaCl, 0.5 ml 0.05 % Tween20) for 60 minutes. Membranes were transferred into hybridization bags and incubated with the primary antibody on a rocker overnight at 4°C. The primary antibodies were diluted in 6ml 5% milk/TBS-T and 60µl 2% sodium azide, see **Table 6** for all primary antibodies and dilutions used.

Table 6: Primary antibodies used in murine and human samples

<i>Antibody</i>	<i>Dilution</i>	<i>Species</i>	<i>Molecular Weight</i>	<i>Merchant</i>
<i>α-SFXN1</i>	1:1000	α-rabbit	34 kDa	Atlas Antibodies; #HPA019543
<i>α-SFXN2</i>	1:500	α-mouse	34 kDa	Sigma-Aldrich; #HPA026834
<i>α-SFXN3</i>	1:1000	α-rabbit	35 kDa	Sigma-Aldrich; #HPA048105
<i>α-SFXN4</i>	1:1000	α-rabbit	34 kDa	Cusabio Antibodies; #CSB-PA744046LA01HU
<i>α-SFXN5</i>	1:5000	α-rabbit	37 kDa	Cusabio Antibodies; #CSB-PA819464LA01HU
<i>α-GAPDH</i>	1:2000	α-mouse	35 kDa	Cell Signaling Technology; #97166
<i>α-Citrate Synthase</i>	1:1000	α-rabbit	45 kDa	Cell Signaling Technology; #14309
<i>α-Calreticulin</i>	1:1000	α-rabbit	55 kDa	Cell Signaling Technology; #12238
<i>α-SHMT2</i>	1:1000	α-rabbit	55 kDa	Sigma Prestige Antibodies; #HPA020549
<i>α-MTHFD2</i>	1:1000	α-mouse	38 kDa	Santa Cruz Biotech; #sc-390708
<i>α-MTHFD1(L)</i>	1:1000	α-rabbit	106 kDa	Cell Signaling Technology; #14998S

Membranes were washed three times using TBS-T for 5 minutes. Subsequently, dilutions of the HPR-linked secondary antibody, anti-rabbit (1:3000; Cell Signaling Technology, 7074) and anti-mouse (1:2500; Cell Signaling Technology, 7076), were made. The membranes were incubated for 60 minutes on a rocker at room temperature. Afterwards, three washing steps of 5 minutes each occurred. To detect the binding of the antibody, membranes were incubated with the Pierce™ ECL™ Western Blotting Substrate (Thermo Scientific; #32106). After a 1-minute long incubation step, the membranes were put into a developing cassette. The developing step occurred in a dark room. CL-XPosure films (Thermo Scientific; #34091) were laid on top of the membranes. The films were exposed to the chemiluminescent signals for different time periods and developed using the Kodak XOMAT 2000 processor. If required, membranes were washed in TBS-T, stripped for 11 minutes using the Restore Western Blot Stripping Buffer (Thermo Scientific; #21059), washed three times for 5 minutes and blocked in 5% milk/TBS-T for 60 minutes. Upon the blocking the membranes were processed as described above. Used membranes were afterwards dried and stored at room temperature.

2.3.4 Semi-quantification of SFXN bands

Developed films were scanned and imported using the Image Studio Lite Ver 5.2 software provided by BioRad. The band intensities were calculated and exported. To quantify the fold change of protein expression, the protein bands of KO samples were normalized to those of the wild type samples. In addition, the samples were normalized to loading control values. The statistical analysis occurred by using GraphPad Prism 8.0. A two-way ANOVA with Dunnett's multiple comparisons test was used. The p-value was set to 0.05. Error bars in the graphs indicate the standard deviation.

2.4 Metabolite profiling using Liquid Chromatography-Mass Spectrometry (LC/MS)

2.4.1 Metabolite Isolation from Murine Tissue Samples

To determine whether any polar metabolic changes are caused by the depletion of SFXN3 the following procedure was designed. 7-8 weeks old SFXN3 29KO, SFXN3 35KO and wild type C57BL6/J mice, with two animals per gender and genotype, were weighed and fasted for 18 hours overnight. A second weight reference was collected in the morning and the mice were re-fed *ad libitum* for 2 hours.

The mice were processed one by one. First, whole blood was collected by restraining the mice and puncturing the meeting point of the retro-orbital and submandibular into the jugular vein using a 4mm animal lancet (Goldenrod).

The blood was drained into ethylenediaminetetraacetic acid (EDTA) pre-treated MiniCollect tubes (Greiner Biolabs; #450474) and kept on ice until all samples were obtained. Subsequently, the mice were euthanized by cervical dislocation. Afterwards, samples were spun down at 3000 rpm for 6 minutes at 4°C. The plasma was transferred into a 1.5ml tube. Metabolites from 10µl of the collected fraction were isolated using 90µl of an acetonitrile-based extraction buffer (75% acetonitrile, 25% methanol, 0.2% formic acid with 909nM of each 17 isotopically labeled amino acids; Cambridge Isotope Laboratories). Samples were vortexed for 10 seconds and spun down at maximum speed for 10 minutes at 4°C. The supernatant was transferred into a new tube and the pelleted insoluble fraction was discarded. Isolated metabolites were dried down using a vacuum centrifuge.

In addition to the plasma, soft tissue was collected as described above. Tissues of interest were brain, kidneys, liver, lungs and the brown fat tissue. Approximately 30mg per tissue were set aside for the Western Blot and the remaining tissue was snap-frozen for the metabolite extraction. Samples were removed from the nitrogen and powdered using a ceramic mortar and pestle on dry ice. Tissue powder was collected into a storage tube and approximately 26-29mg were weighed into a 2ml microcentrifugation tube. For the metabolite extraction only powders of the brain and the kidney were used. 1ml of a methanol-based extraction buffer (80% methanol, 20% water and 500nM labeled isotope standards; Cambridge Isotope Laboratories) was added to the powder and vortex samples for 10 min at 4°C. Samples were spun down at maximum speed for 10min at 4°C, supernatants were moved to new 1.5ml tubes, dried down and stored at -80°C.

The same procedures as for the SFXN3 KO mice was performed. Four 7-week-old female heterozygous SFXN1 (SFXN1 Het) and four 7-week-old female C57BL6/J mice were used. The tissues collected were the brain, liver, kidney, spleen and brown fat tissue. In addition to the plasma, only the metabolites from 29mg powdered liver samples were extracted, dried down and stored.

2.4.2 Sample Preparation and Analysis

Prior to the samples being run, dried down metabolites were resuspended in 100µl LC/MS grade water (Fischer Chemicals; #168696). The suspension was transferred into LC/MS vials (Thermo Fischer; vials - #C4000-11, caps – C5000-54B) and ran with corresponding controls using a Thermo Scientific QExactive Orbitrap. Metabolite profiling was performed as described by Birsoy *et al* and Chen *et al* [79], [80]. Briefly, amino acids were normalized to their respective standards and purine synthesis intermediates were normalized to the internal glutamate standard. The KO sample values were normalized to the wild type samples to quantify a potential fold change. Data normality was assessed by the D'Agostino & Pearson test as well as the Shapiro-Wilk test.

Two-tailed t-tests (parametric or non-parametric) were applied and the p-value was set to 0.05. Error bars in the graphs indicate the standard deviation. Depending on the results of the normality test, either the Kruskal-Wallis test with Dunn's multiple comparisons test or a one-way ANOVA test with Dunnett's multiple comparisons test were used to analyze the data from SFXN3 animals. The SFXN1 Het raw peak values were normalized to the wild type samples to quantify a potential fold change. For the statistical analysis, either the Unpaired two-tailed t-tests (parametric, t test with Welch's correction or non-parametric, Mann-Whitney test) were applied.

2.5 RNA seq and Graphic Design

For the analysis of predicted SFXN1-5 expressions, previously published RNA sequencing data sets were used. An Expression Atlas, containing several different RNA data sets, was published by Papatheodorou *et al* as a project of the European Molecular Biology Laboratory, European Bioinformatics Institute [81]. Data on SFXN1-5 expression was obtained from the human GTEx and FANTOM5 RNA seq and the FANTOM murine RNA seq (<https://www.ebi.ac.uk/gxa/home>). The expressions of SFXN1-5 in different tissues were manually picked and entered in GraphPad Prism 8.0 to create an expression heatmap. Data sets on the human proteome and the expression of the different SFXN isoforms were obtained through the Human Proteome Map (<https://www.humanproteomemap.org/download.php>). Values were again manually sorted and entered in GraphPad Prism 8.0 to create heatmaps. The single-cell RNA expression data sets of SFXN1, SFXN3 and SFXN5 in the non-myeloid brain were obtained from the *Tabula Muris* platform (<https://tabula-muris.ds.czbiohub.org/images/All-facs-tissue-tsne.png>) [82].

Considering the graphic design presented, all figures without addition of paper references were made by the author using the BioRender graphics software.

3 Results

3.1 Sideroflexin Expression in Humans and Mice

The processing of the FANTOM5 RNA sequencing (RNAseq) data set has revealed that SFXN1 is likely the predominantly expressed isoform, with the highest transcript per minute (TPM) scores in the brain, spinal cord, kidney and the heart. Furthermore, SFXN4 was identified to be of a similar expression across several tissue types, as shown in **Figure 5A**.

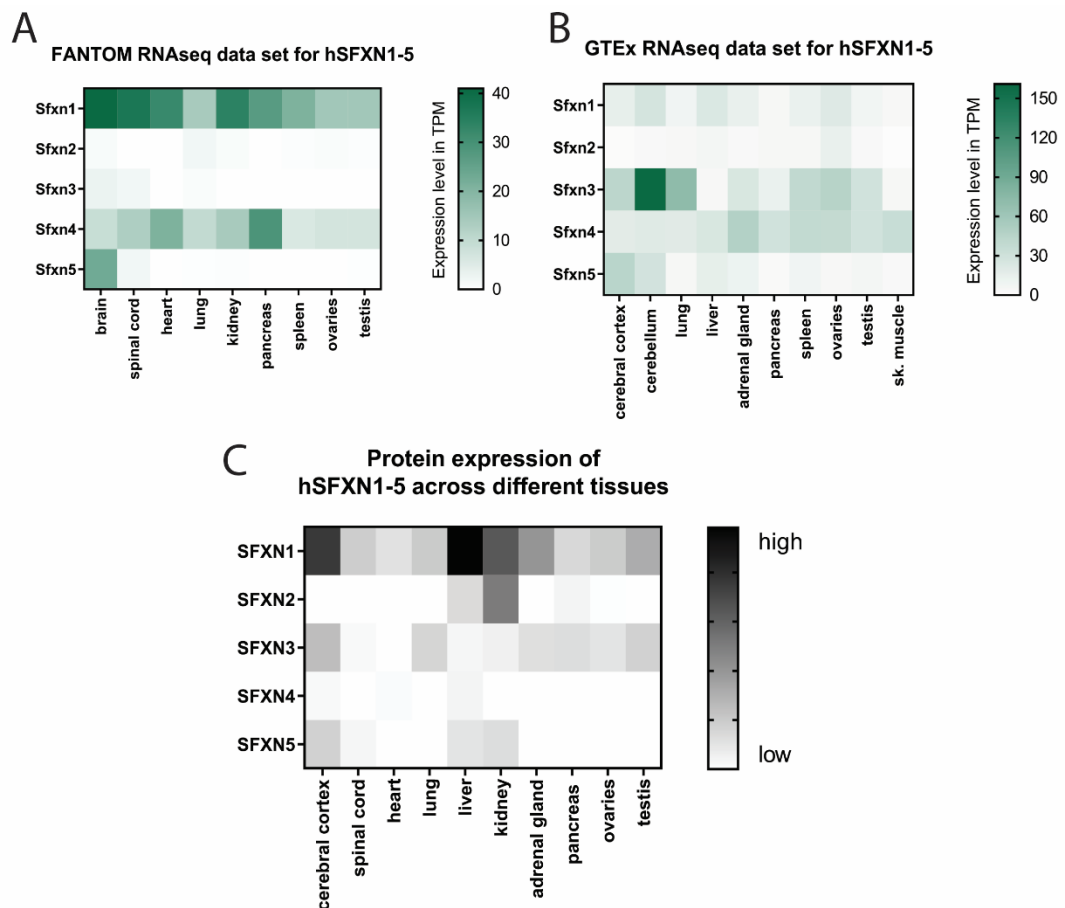


Figure 5: SFXN1 is likely the predominantly expressed isoform in human tissue samples.

A: Generated heatmap of the SFXN1-5 expression levels in different adult human tissues such as, brain, spinal cord, heart, lung, kidney, pancreas, spleen, ovaries and testis. Expression levels were quantified as TPM (transcripts per minute). The heatmap was generated using the FANTOM5 RNA seq data set (range: 0-41 TPM). B: Heatmap of SFXN1-5 transcription levels in the human cerebral cortex, cerebellum, lung, liver, adrenal gland, pancreas, spleen, reproductive organs and skeletal muscle. The heatmap was generated using the GTEx RNA seq data set (range: 0-161 TPM). C: Protein expression levels of human SFXN1-5 in cerebral cortex, spinal cord, heart, lung, liver, kidney, adrenal gland, pancreas and the reproductive organs.

Interestingly, the expression levels of SFXN2 and SFXN3 were marginal, whereas SFXN5 is predicted to be highly expressed in the human brain. The GTEx data set presents SFXN1 and SFXN4 to be also expressed in other highly metabolically tissues such as the liver and adrenal gland. Moreover, this data set shows SFXN3 to be highest expressed isoform in the cerebellum followed by the lung and the cerebral cortex, to be noted in **Figure 5B**. SFXN1 was shown to be highly expressed in human samples of the liver, kidneys and cerebral cortex, whereas its redundant homologue, SFXN3, had the highest levels in the cortex and lungs, shown in **Figure 5C**. Expression patterns shown for SFXN5 correlate with those of SFXN1. SFXN2 was predominantly detected in the kidneys and the liver, where SFXN4 was only minimally expressed in the human liver, cortex and heart.

In order to study the role of SFXNs, the comparability of the murine and the human organism was assessed. **Figure 6A** shows a global expression of the different SFXN homologues in the murine organism, collected during the FANTOM project. SFXN1 transcript levels were the highest in the murine liver, kidneys, adrenal gland and pancreas. In contrast to the human data set, a murine heart does not express SFXN1. SFXN2 revealed the same pattern as in the human FANTOM5 RNA seq data set. The lung and components of the nervous system are the main expression sites of SFXN3, which was also seen in the human sequencing results. Strikingly, SFXN5 was predicted to have the highest expression level in the components of the nervous system. Furthermore, this homologue revealed to also have substantial transcript levels in the murine liver, kidney adrenal gland and pancreas.

To verify the RNA sequencing results, murine tissue samples were collected, and the native protein expression was assessed via immunoblotting. All five SFXN homologues are likely expressed across different murine tissues. Moreover, SFXN1 is to be identified as the predominantly expressed isoform. The highest levels of SFXN1 were found in the kidney followed by the liver and the cerebral cortex. Across these tissues, only heart and skeletal muscle were lacking SFXN1, as depicted in **Figure 6B**. SFXN3 was predominantly expressed in the cerebral cortex, the cerebellum and spinal cord. Marginal amounts were detected in the liver and brown fat. In contrast to the presented RNA seq transcript levels, SFXN3 was not detected in the murine lung samples. SFXN4 was identified mainly in the liver followed by a lower expression in the brown fat and the nervous system. The expression of SFXN5 in the nervous system correlates with the murine RNA sequencing data set. Interestingly, SFXN5 is expressed in the nervous system in a duplet, revealing two different isoforms. SFXN5 was not detected in the heart and skeletal muscle. Other tissues used for the experiment expressed either the long or the short isoform of this protein. Due to the different proteome of the chosen tissue, three different house-keeping proteins were assessed; GAPDH, citrate synthase and calreticulin.

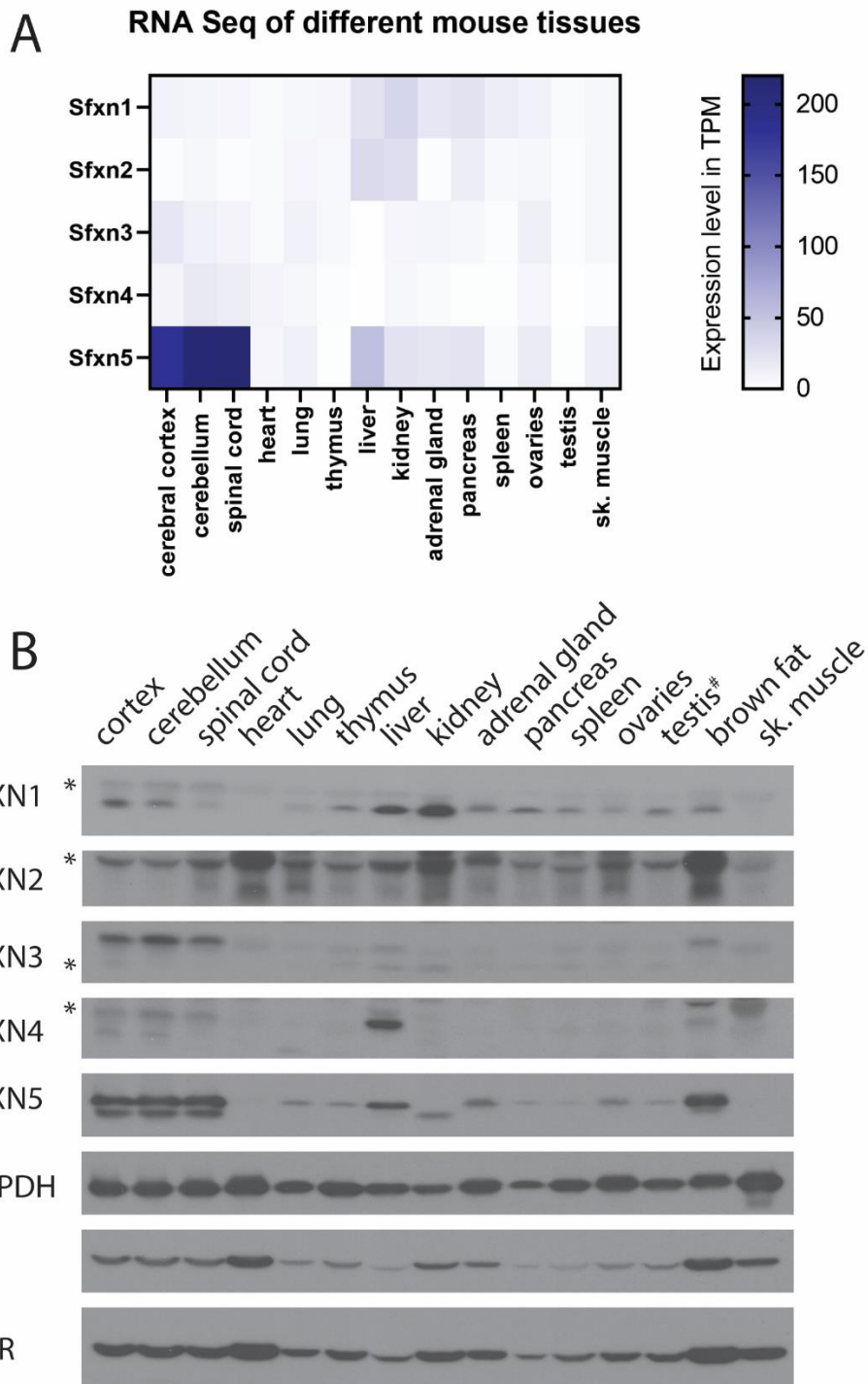


Figure 6: Global SFXN expression in the murine system reveals SFXN1 as the predominantly expressed homologue. A: Generated heatmap of the SFXN1-5 expression levels in different adult murine tissues. Expression levels were quantified as TPM (transcripts per minute). The heatmap was made using the FANTOM5 RNA seq data set (range: 0-220 TPM). B: SFXN1-5 expression across different murine tissues. Antibodies used SFXN1-5 (Sideroflexin 1-5); GAPDH (Glyceraldehyde 3-phosphate dehydrogenase), CS (citrate synthase), CalR (Calreticulin). Protein amount was normalized to 40ng per lane. # = sample used form another animal; * = unspecific bands

Figure 7B and **Figure 8B** show the Next Generation Sequencing results for SFXN1 and SFXN3 animals, respectively. The sequencing results show an 8 base pair deletion in exon 8 of the *Sfxn1* gene. **Figure 7B** shows a representative sequencing result of a heterozygous (SFXN1 Het) and a wild type (WT) animal. No homozygous SFXN1 KO animals were registered. **Figure 8B** presents the sequencing results of the SFXN3 mice. Two different knockout alleles were detected, a homozygous 29 base pair (29KO), a homozygous 35 base pair (35KO) deletion as well as a 29 and 35 base pair KO (29/35KO).

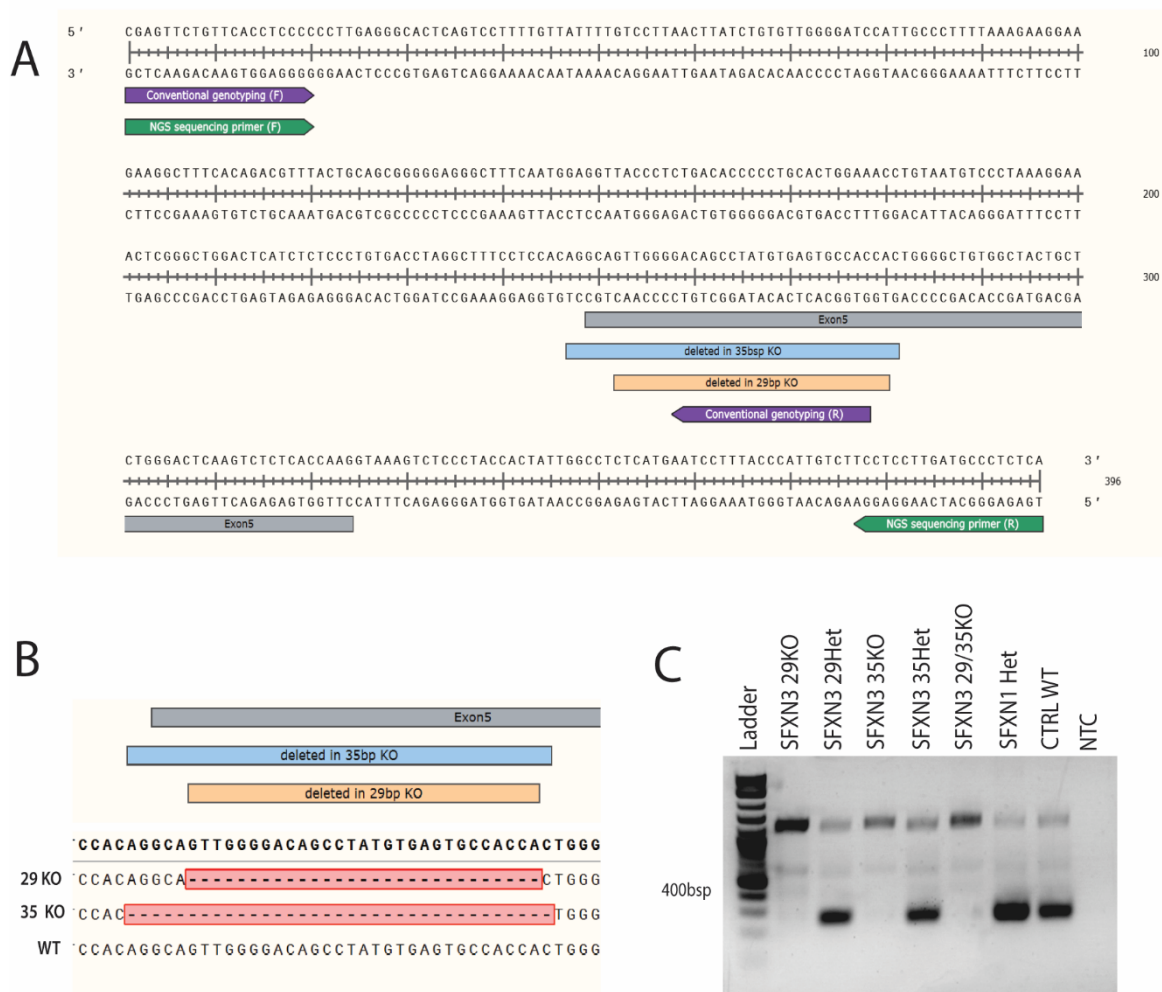


Figure 8: Genotyping reveals a successful deletion in SFXN3. A: Primer pairs designed to flank the cutting site of the SFXN3 sgRNA used for the creation of the KO (green: NGS sequencing primers; purple: Conventional genotyping primers). B: Next Generation Sequencing results are aligned with a NCBI genomic sequence of SFXN3. The genotyping results reveal a 29 and 35 base pair deletion in SFXN3. The alignment was made using the SnapGene Software. C: Representative PCR genotyping gel of SFXN3 animals. A positive control for the wild type allele is indicated (CTRL WT). NGS verified mice were used as controls for the knockouts (SFXN3 29KO, SFXN3 35KO, SFXN3 29/35KO) and heterozygotes (SFXN3 29Het, SFXN3 35Het). NTC indicates the negative control.

Figure 7C and **Figure 8C** show representative PCR-based genotyping results from SFXN1 and SFXN3 test-litters. In both cases, primers were designed in such a way that only the wild type allele is amplified and appears as band on an 4% agarose gel. To test the newly designed primers for SFXN1 and SFXN3, animals with NGS confirmed genotypes were used. SFXN1 appears at a size of 369 base pairs in heterozygous and wild type genotyping samples, **Figure 7C**. As a positive control, indicating a knockout, one of the first-generation animals was used. Due to the short deletions in SFXN1, the PCR results were verified by Transnetx. Heterozygous or wild type SFXN3 bands appear at a size of 278 base pairs, as shown in **Figure 8C**. The animals with a 29/35KO were not used for further experiments.

3.3 Phenotypic Characterization of SFXN1 and SFXN3 KO Mice

Backcrossing of SFXN1- and SFXN3-CRISPR/Cas9 to wild type C57BL6/J mice resulted in the establishment of heterozygous breeding populations. Heterozygous animals were used to establish pure knockout strains. The monitoring of the respective breeding revealed the same frequency of litters being born. Moreover, the numbers of neonates were in both cases on average 5 animals. At weaning, no SFXN1 KO mice resulted from heterozygous breedings, as shown in **Figure 9A**. A comparison between the counted neonates on the day of birth and the number of genotyped mice revealed a trend indicating that SFXN1 KO mice may not be able to survive to adulthood, **Figure 9B**. A closer monitoring regime of SFXN1 litters revealed a trend towards a higher mortality rate of neonates. Over the course of 6 litters an average of 1.4 neonates did not survive until the point of weaning. Such trends were not seen in SFXN3 litters, **Figure 9C**. As a part of general phenotypic characterization, blood glucose levels of SFXN1 Het, SFXN3 29KO and wild type mice were measured. No significant changes were noted after an 18 hours long fasting window in a cohort of 4 male age-matched animals, **Figure 9D**. The change in murine body mass before and after change is to be seen in **Figure 9E**. No significant changes were noted. Lastly, the body mass of all strains and the wild type control was tracked over the course of six weeks to assess the growth process of SFXN1 and SFXN3 mice in comparison to wild type animals. Male mice are shown in **Figure 9F**, female in **Figure 9G**. Both female and male SFXN3 29KO as well as female and male SFXN1 Het animals gained weight in a similar pace as the age-matched controls.

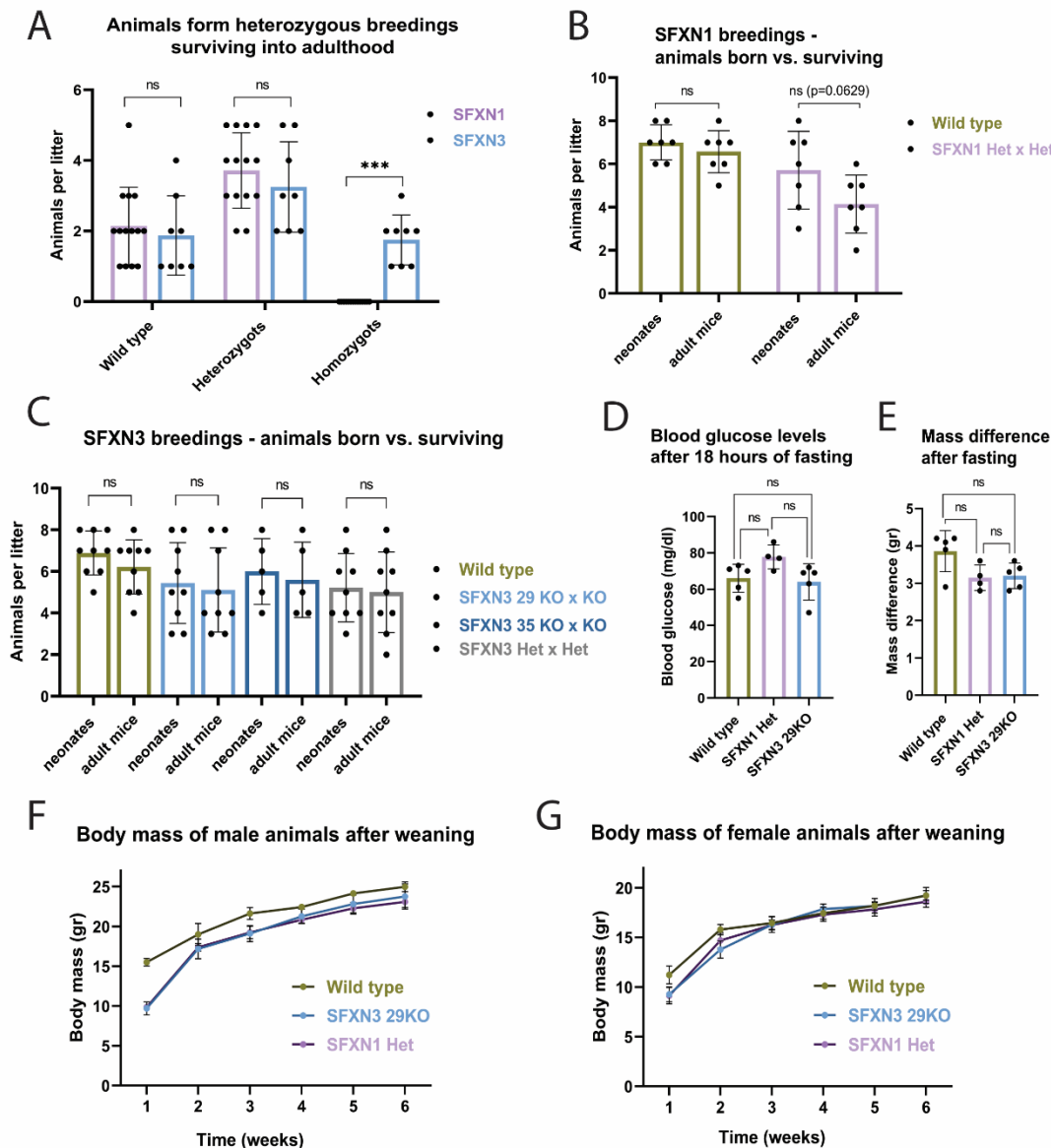


Figure 9: Basic characterization of SFXN1 and 3 mice. A: Distribution of genotypes in weaned adult mice. A lack of SFXN1 KO animals is to be noted (mean \pm SD; n of SFXN1 Het x Het litters=14; n of SFXN3 Het x Het litters=8; Two-tailed Mann-Whitney test; p-value=0.05; ***p \leq 0.0002). B: Ratio of SFXN1 neonates from heterozygous breedings surviving until adulthood (mean \pm SD; n of litters=7; Unpaired two-tailed t test with Welch's correction; p-value=0.05). C: Ratio of SFXN3 neonates surviving until adulthood (mean \pm SD; n of litters=9; Unpaired two-tailed t test with Welch's correction; p-value=0.05). All breeding schemes were included. D: Measurements of blood glucose levels in male animals after 18 hours of fasting (mean \pm SD; n=4; ordinary one-way ANOVA with Tukey's multiple comparisons test; p-value=0.05). E: Body mass difference of male animals 26 hours before and after an 18 hour fasting period (mean \pm SD; n=4; Kruskal-Wallis with Dunn's multiple comparisons test; p-value=0.05). F: Body mass of male SFXN1 Het, SFXN3 29KO and wild type animals over the course of six weeks (mean \pm SD; n=5 per genotype). G: Body mass of female SFXN1 Het, SFXN3 29KO and wild type animals over the course of six weeks (mean \pm SD; n=5 per genotype).

A trend in phenotype was observed in SFXN1 breedings. **Figure 10A** shows two litters from different parent animals. Fleming *et al* previously described the phenotype of transient anemia in animals lacking SFXN1. This resulted in a paler appearance of neonates when compared to wild type or heterozygous litter mates [55]. A similar phenotype is also to be expected in the newly established SFXN1 KO strain. Indeed, the affected animals are paler in comparison to their mates in our hands as well, indicated by the yellow arrows in **Figure 10A**. These animals did not survive the first 24 hours after birth.

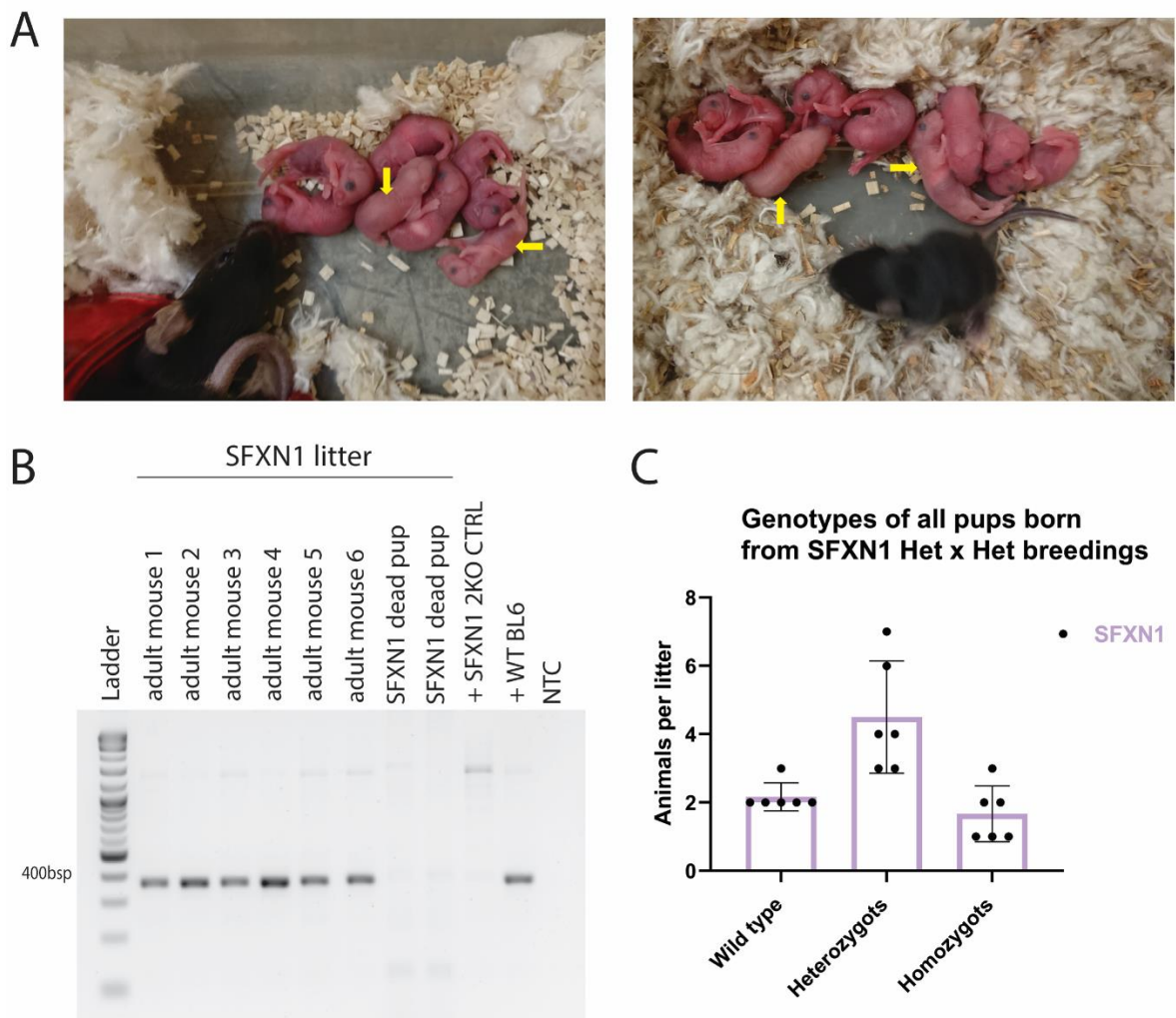


Figure 10: Characterization of SFXN1 heterozygous breeding litters. A: Representative images of SFXN1 litters on the day of birth. Paler animals are indicated by the yellow arrow. B: Genotyping gel of a complete SFXN1 litter including pups which were found dead and their litter mates. Deletions were verified by Transnetyx. C: Distribution of the genotypes detected in six consecutive litters revealing the expected Mendelian inheritance of a heterozygous breeding (mean \pm SD).

Tails of the dead pups were collected and genotyped revealing the homozygous 8 base pair deletion in exon 8 of SFXN1 in the dead neonates, as seen in **Figure 10B**. A distribution of the genotypes in SFXN1 neonates can be seen in **Figure 10C**. The expected Mendelian inheritance of a heterozygous breeding should result in a genotypic ratio of 1:2:1 (wild type to heterozygous to homozygous animals) and a phenotypic ratio of 3:1 [83]. The phenomenon was tracked over six different litters. As presented in **Figure 10C** the Mendelian law of segregation is given in the monitored SFXN1 litters. These results indicate that SFXN1 loss is not detrimental for embryonal development.

3.4 The Loss of a Functional SFXN1 Allele Leads to a Decrease in SFXN1 Protein Levels and Reveals Changes in the Murine Metabolism

We performed immunoblotting of the cortex, cerebellum, liver, kidney, spleen and brown fat, to determine whether the heterozygous 8 base pair deletion of SFXN1 has an effect on the expression of the protein. Indeed, the loss of one functional allele results in a 50% reduction of SFXN1 protein level as expected. Furthermore, it was assessed whether this results in any compensatory changes in levels of other Sideroflexin homologues **Figure 11A**. The immunoblotting of the murine liver was repeated in a larger cohort of samples. The results, shown in **Figure 11B**, confirmed the replicability of the data presented in **Figure 11A**.

The largest numbers of mitochondria were found in the liver due to the functionality of the organ [3]. In our hand, SFXN1 is highly expressed in the liver, **Figure 6**. In addition, SFXN1 was predicted to be important in erythrocytes as well as other blood cells [20]. Therefore, we hypothesized that the loss of one functional allele will have an effect on the metabolism of the animals. **Figure 11B** verifies the decrease in SFXN1 protein levels in the SFXN1 Het cohort when compared to wild type. Again, no alterations in other SFXN homologue expression could be detected in liver samples.

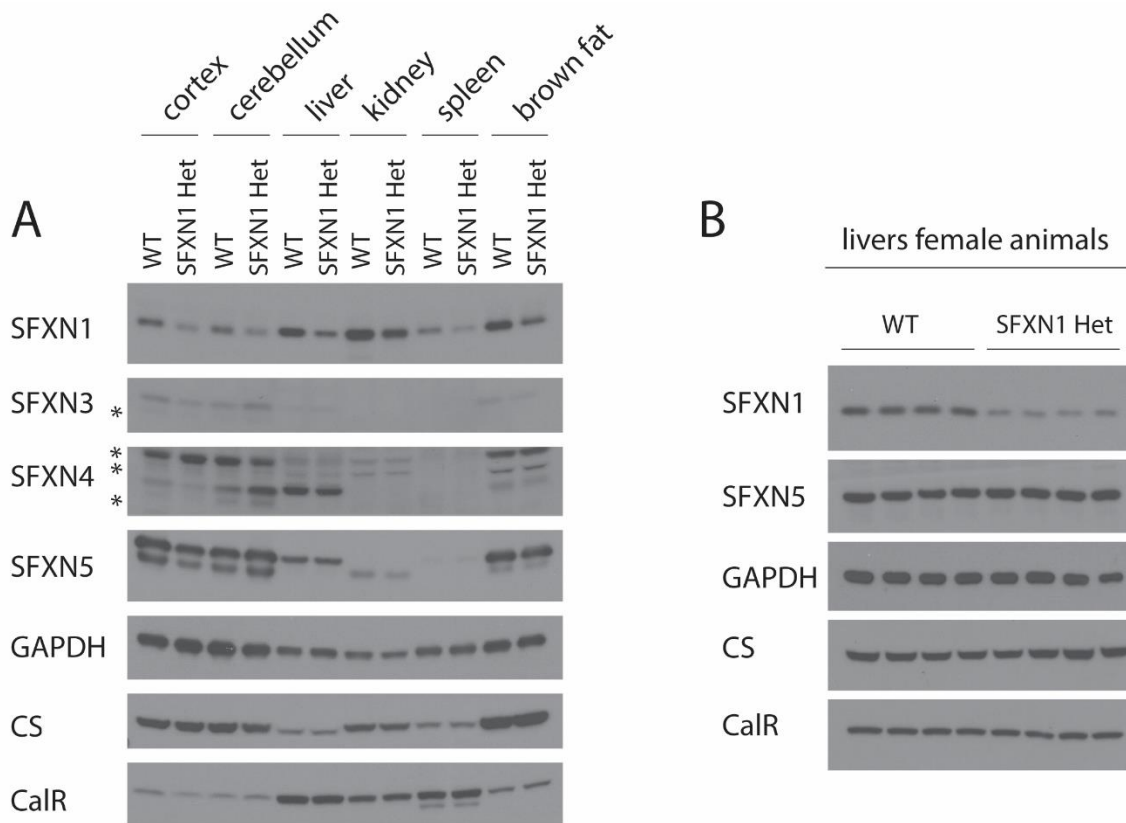


Figure 11: The loss of a functional SFXN1 allele reveals a decrease in SFXN1 protein levels.

A: A loss of a functional SFXN1 copy accounts for 50% of protein levels in tissues of age-matched female animals. Antibodies used SFXN1-5 (Sideroflexin 1-5); GAPDH (Glyceraldehyde 3-phosphate dehydrogenase), CS (citrate synthase), CalR (Calreticulin). B: The 50% loss of protein levels in SFXN1 Het livers is replicable. Age-matched SFXN1 Het wildtype animals were used (n=4 per genotype). Antibodies used SFXN1, 5 (Sideroflexin 1 and 5); GAPDH (Glyceraldehyde 3-phosphate dehydrogenase), CS (citrate synthase), CalR (Calreticulin). Protein amount was normalized to 40ng per lane for both experiments. * = unspecific bands

By losing a copy of SFXN, serine transport into the mitochondrion should be impaired. The amino acid profiling is expected to reveal increased serine and decreased glycine amounts in SFXN1 Het sample when compared to wild type [20]. The profiling did not reveal significant changes in serine and glycine levels. However, a trend towards serine accumulation could be detected in the samples from heterozygous animals. Amino acids such as phenylalanine, methionine, tyrosine and proline were significantly decreased in SFXN1 livers, shown in **Figure 12A**. Plasma samples revealed similar trends for serine. However, only the significant decrease in tyrosine was consistent with the results seen in the liver, as seen in **Supplementary Figure 1A**. The plasma samples also reveal a significant increase in histidine and valine levels.

Due to the changes detected in the amino acid levels in the liver, we focused on metabolites related to the one-carbon metabolism. Nucleotide synthesis should be defective if SFXN1 is lost leading to alterations in the one-carbon metabolism. Especially purine synthesis intermediates, such as AICAR, inosine, guanosine or xanthine should indicate changes [20]. A trend of increased AICAR levels in the SFXN1 het samples was noted. Significant increase in inosine monophosphate levels as well as decrease in inosine and guanosine were detected, as depicted in **Figure 12C**. Due to the high numbers of mitochondria in the liver, elements of mitochondrial metabolism dependent on one-carbon units were analyzed. An overall trend in decreased mitochondrial metabolite levels were noted. Especially, the changes in urea cycle intermediates were significant in our hands, to be seen in **Figure 12D**. Alterations in TCA cycle intermediates, should have an impact on the transamination processes, required to produce *de novo* amino acids [23]. A striking decrease in glutamate levels was observed in SFXN1 Het animals, shown in **Figure 12B**.

Lysine is an essential amino acid required for methylation processes, fatty acid oxidation and the urea cycle [8], [84]. Both pathways are impacted by the loss of enough one-carbon supply. Resulting, we hypothesize that lysine levels as well as its synthesis intermediates will be impacted. The analysis of lysine synthesis intermediates revealed decreased metabolite levels in SFXN1 Het animal, see **Figure 12E**. These findings support the significance of the changes detected in urea cycle intermediates in **Figure 12D**.

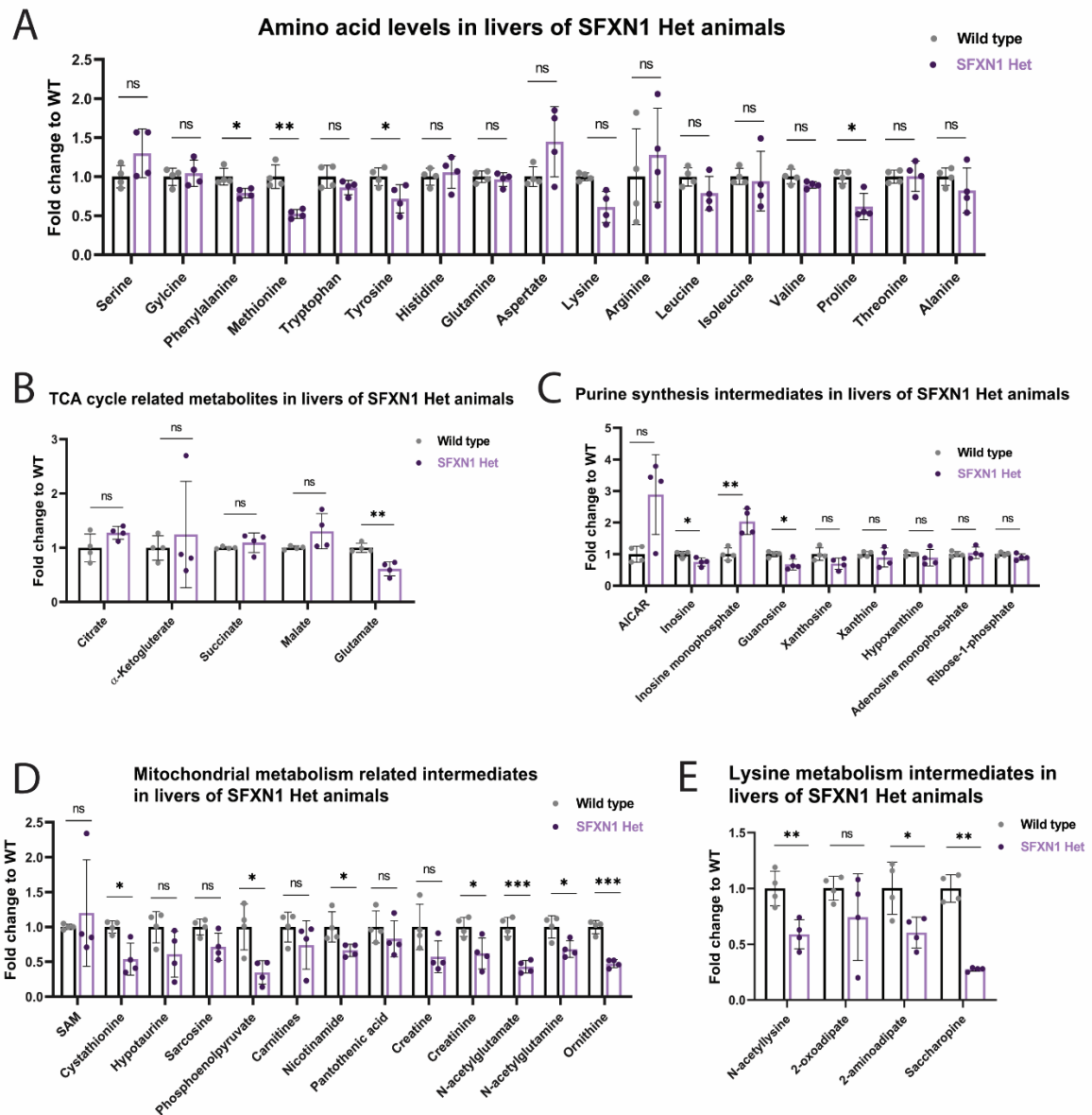


Figure 12: The loss of a functional SFXN1 allele leads to alterations of the murine metabolism.
 A: Metabolic profiling of amino acids in SFXN1 Het liver samples (mean \pm SD; n=4 per genotype; Unpaired two-tailed t-tests with Welch's correction or Mann-Whitney test; *:p \leq 0.05, **:p \leq 0.001). B: Metabolic profiling of TCA cycle related metabolites in SFXN1 Het liver samples (mean \pm SD; n=4 per genotype; Unpaired two-tailed t-tests with Welch's correction or Mann-Whitney test; **:p \leq 0.001). C: Metabolic profiling of purine synthesis intermediates in SFXN1 Het liver samples (mean \pm SD; n=4 per genotype; Unpaired two-tailed t-tests with Welch's correction or Mann-Whitney test; *:p \leq 0.05, **:p \leq 0.001). D: Metabolic profiling of mitochondrial metabolism related molecules in SFXN1 Het liver samples (mean \pm SD; n=4 per genotype; Unpaired two-tailed t-tests with Welch's correction or Mann-Whitney test; *:p \leq 0.05, **:p \leq 0.001). E: Metabolic profiling of lysine metabolism intermediates in SFXN1 Het liver samples (mean \pm SD; n=4 per genotype; Unpaired two-tailed t-tests with Welch's correction or Mann-Whitney test; **:p \leq 0.001).

3.5 The Loss of SFXN3 Alters SFXN1 Expression in the Brain but not in the Kidney or Liver

SFXN3 was shown to be expressed in the nervous system of adult mice, **Figure 6**. The loss of SFXN3 has no impact on the SFXN5 protein levels, which is a further Sideroflexin homologue found in the brain. Strikingly, an effect on SFXN1 protein levels was noted, see **Figure 14A**.

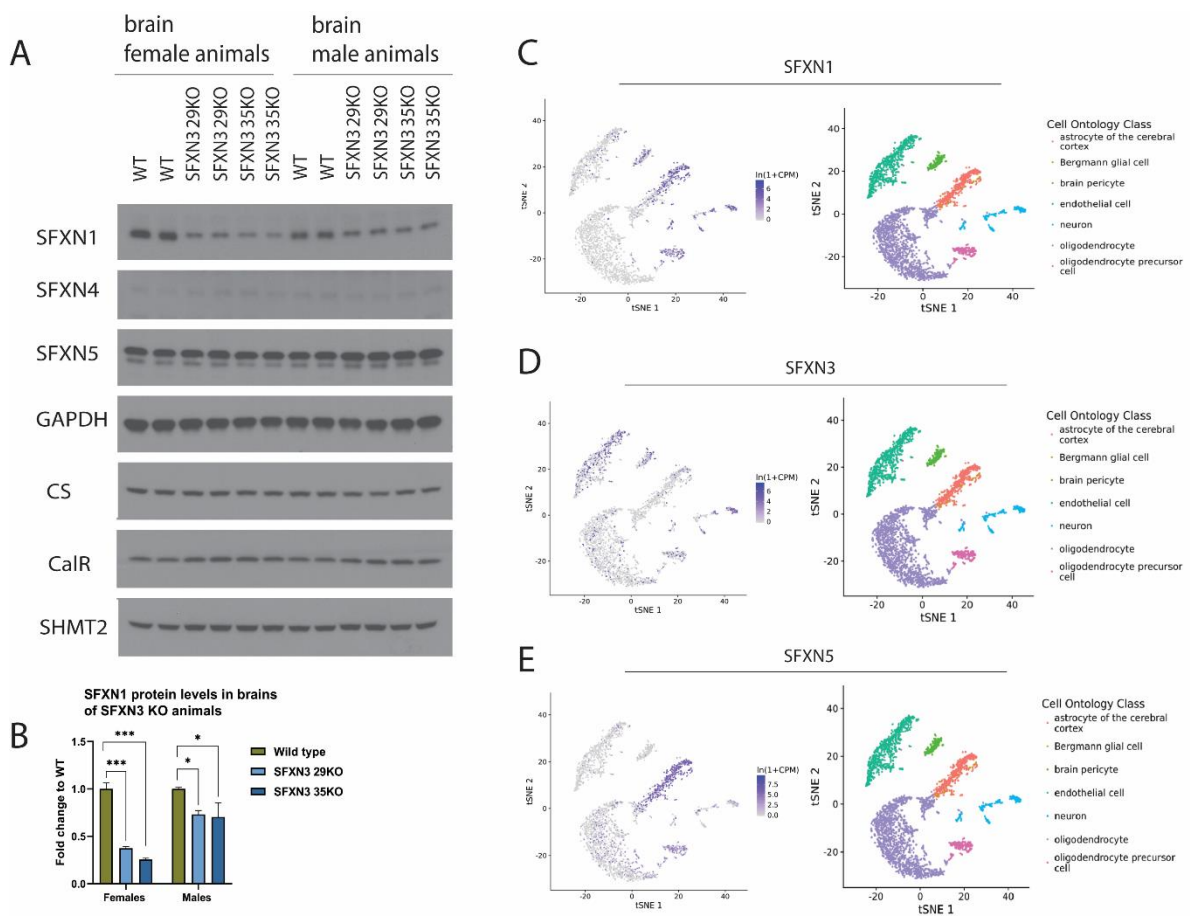


Figure 13: Loss of SFXN3 alters SFXN1 expression in the murine brain. A: SFXN1 expression in SFXN3 knockout brains. SFXN1 levels alter when compared to wild type samples. Antibodies used SFXN1, 4, 5 (Sideroflexin 1, 4, 5); GAPDH (Glyceraldehyde 3-phosphate dehydrogenase), CS (citrate synthase), CalR (Calreticulin), SHMT2 (Serine hydroxymethyltransferase 2). Protein amount was normalized to 40ng per lane. B: Signal quantification of SFXN1 bands. Bands were normalized to GAPDH and the fold change was calculated by normalizing to wild type (mean \pm SD; n=2; Two-way ANOVA with Dunnett's multiple comparisons; *: $p \leq 0.05$; ***: $p \leq 0.0001$). C: t-SNE cluster of single-cell RNA expression data of SFXN1 in the non-myeloid brain (*Tabula Muris*). D: t-SNE cluster of single-cell RNA expression data of SFXN3 in the non-myeloid brain (*Tabula Muris*). E: t-SNE cluster of single-cell RNA expression data of SFXN5 in the non-myeloid brain (*Tabula Muris*).

The quantification of SFXN1 expression in SFXN3 KO brains revealed a significant decrease, when compared to the wild type. The effect of SFXN3 loss is more striking in the female brains, **Figure 14B**. No differences were noted between the male animals. The single cell RNA sequencing revealed that SFXN1 is predominantly found in clusters of cerebral cortex astrocytes, neurons, Bergmann glia and oligodendrocyte precursors located in the non-myeloid brain, shown in **Figure 14C**. **Figure 14D** presents the predicted localization of SFXN3 in neurons, pericytes of the brain and endothelial cells as well as lowly expressed in oligodendrocytes. SFXN5 is predicted to be expressed mainly in astrocytes of the cerebral cortex. **Figure 14E** additionally shows the expression of SFXN5 in precursor and mature oligodendrocytes.

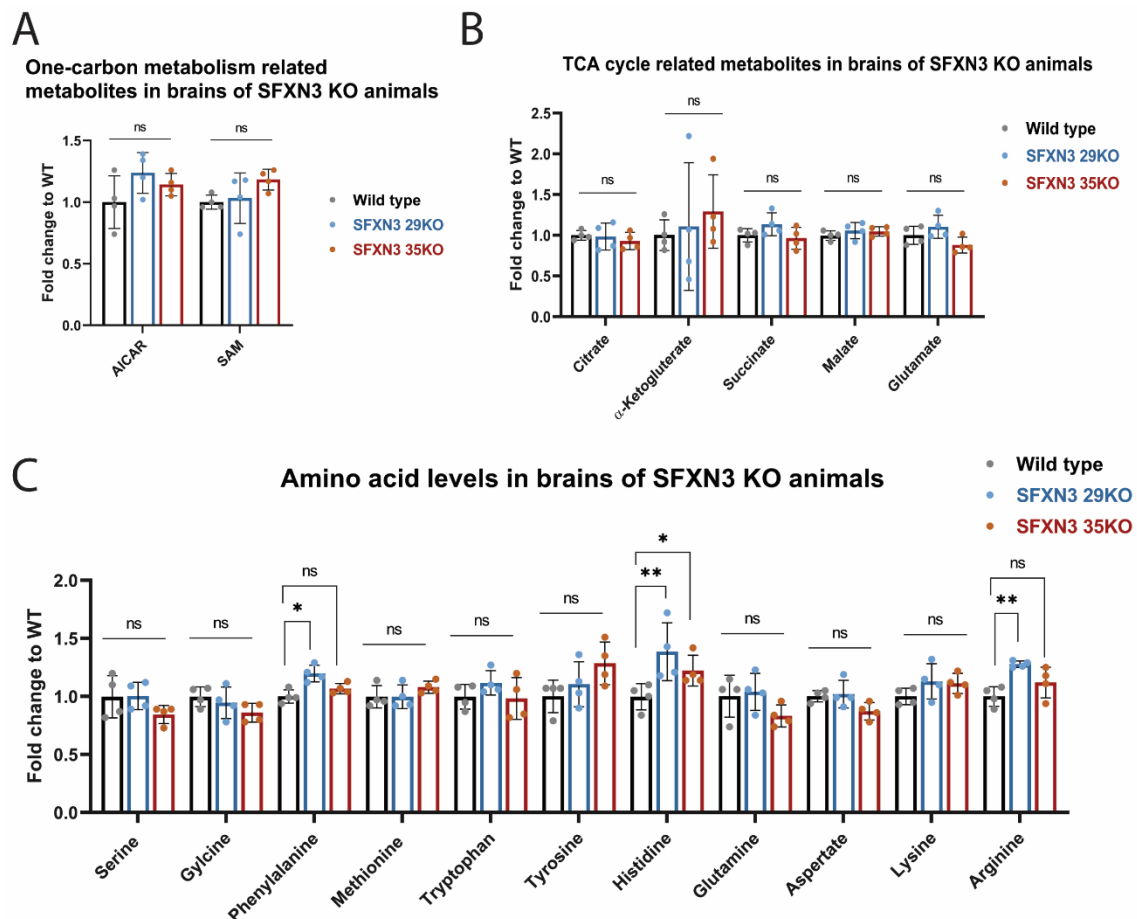


Figure 14: The loss of SFXN3 does not alter serine and glycine levels in the murine brain. A: Metabolic profiling of one-carbon metabolism related intermediates in SFXN3 knockout brain samples (mean \pm SD; n=4 per genotype; Kruskal-Wallis with Dunn's multiple comparisons test; p-value=0.05). B: Metabolic profiling of TCA cycle intermediates in SFXN3 knockout brain samples. (mean \pm SD; n=4 per genotype; ordinary one-way ANOVA with Tukey's multiple comparisons test or Kruskal-Wallis with Dunn's multiple comparisons test; p-value=0.05). C: Metabolic profiling of amino acids in SFXN3 knockout brain samples. (mean \pm SD; n=4 per genotype; ordinary one-way ANOVA with Tukey's multiple comparisons test or Kruskal-Wallis with Dunn's multiple comparisons test; *:p \leq 0.05, **:p \leq 0.001).

The immunoblot revealed changes which were followed up by LC/MS-based metabolomics of the brain. If the serine transport into the mitochondrion would be impaired, an amino acid profiling should reveal increased serine and decreased glycine amounts in the knockouts [20]. Furthermore, an accumulation of purine intermediates should occur. AICAR levels are not increased in SFXN3 animals in comparison to wild type, shown in **Figure 14A**.

Metabolic profiling of the TCA cycle was performed to assess changes caused by the hypothesized defective serine uptake. Metabolites such as α -ketoglutarate are important for serine synthesis through transamination [23]. If the serine transporter is defective it is expected that the TCA cycle would need to synthesize more α -ketoglutarate to generate serine. The metabolomic analysis of the brain did not reveal significant changes of α -ketoglutarate levels in SFXN3 knockout brains when compared to wild type, **Figure 14B**.

The profiling of amino acids did not reveal changes in serine and glycine levels. In contrast, significant changes were noted in amino acids such as phenylalanine, histidine and arginine, depicted in **Figure 14C**. Histidine levels were significantly increased in SFXN3 KO animals of both alleles in comparison to wild type. The increase in phenylalanine and arginine are specific to the SFXN3 29KO genotype and are thus considered as artefacts.

SFXN3 is very lowly expressed in kidney and liver whereas SFXN1 is the predominant isoform in these tissues. It is hypothesized that SFXN1 would not alter its protein levels in these tissues, since it is not required to compensate for loss of another homologue. Thus, an immunoblot of these tissues was performed revealing that changes in SFXN1 levels are specific to the brain, as shown in **Figure 15A**. The metabolic profiling of TCA cycle intermediates, shown in **Figure 15B**, as well as amino acids, **Figure 15C**, did not show significant in the presented metabolites.

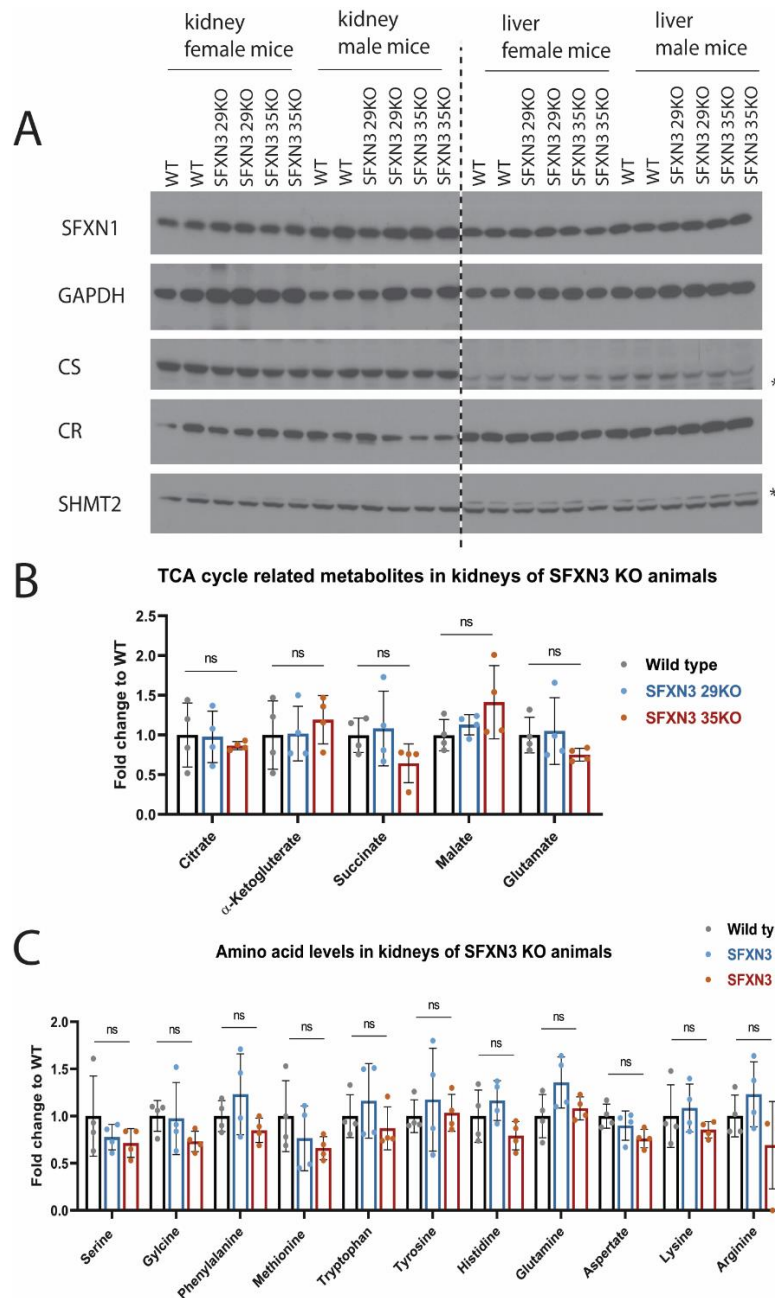


Figure 15: The changes in SFXN1 expression levels of SFXN3 KO mice are specific to the brain.

A: The expression of SFXN1 in SFXN3 KO murine kidney and liver tissues remains at wild type levels. Antibodies used SFXN1 (Sideroflexin 1); GAPDH (Glyceraldehyde 3-phosphate dehydrogenase), CS (citrate synthase), CaR (Calreticulin), SHMT2 (Serine hydroxymethyltransferase 2). Protein amount was normalized to 40ng per lane. * = unspecific bands B: Metabolic profiling of TCA cycle intermediates in SFXN3 KO kidney samples. (mean \pm SD; n=4 per genotype; ordinary one-way ANOVA with Tukey's multiple comparisons test or Kruskal-Wallis with Dunn's multiple comparisons test; p=0.05). C: Metabolic profiling of amino acids in SFXN3 KO kidney samples. (mean \pm SD; n=4 per genotype; ordinary one-way ANOVA with Tukey's multiple comparisons test or Kruskal-Wallis with Dunn's multiple comparisons test; p=0.05).

3.6 Investigating the Role of Sideroflexins in Lymphoma

Both increased serine *de novo* synthesis rates, and an increased production of one-carbon units are a characteristic for cancer metabolism. Enzymes of the mitochondrial one-carbon metabolism such as, SHMT2 and MTDHFD2 were shown to be overexpressed in cancer samples [71], [72]. Thus, it is likely that SFXN1 may be overexpressed too as an upstream target of the one-carbon pathway.

Figure 16 presents data collected from 10 cancer patients and 5 control patients. SFXN1 is upregulated in all cancer samples. However, three out of five negative controls show a similar overexpression. This pattern is similar across all SFXN homologues. SHMT2 is notably overexpressed in four out of five NOS lymphoma and three out of five DLBC lymphoma samples. As for SFXN1, a similar overexpression of SHMT2 can also be noticed in three tonsil samples. The overexpression of MTHFD1L is however conserved to lymphoma samples solely. This result indicates a specific upregulation of the downstream component of the mitochondrial one-carbon metabolism.

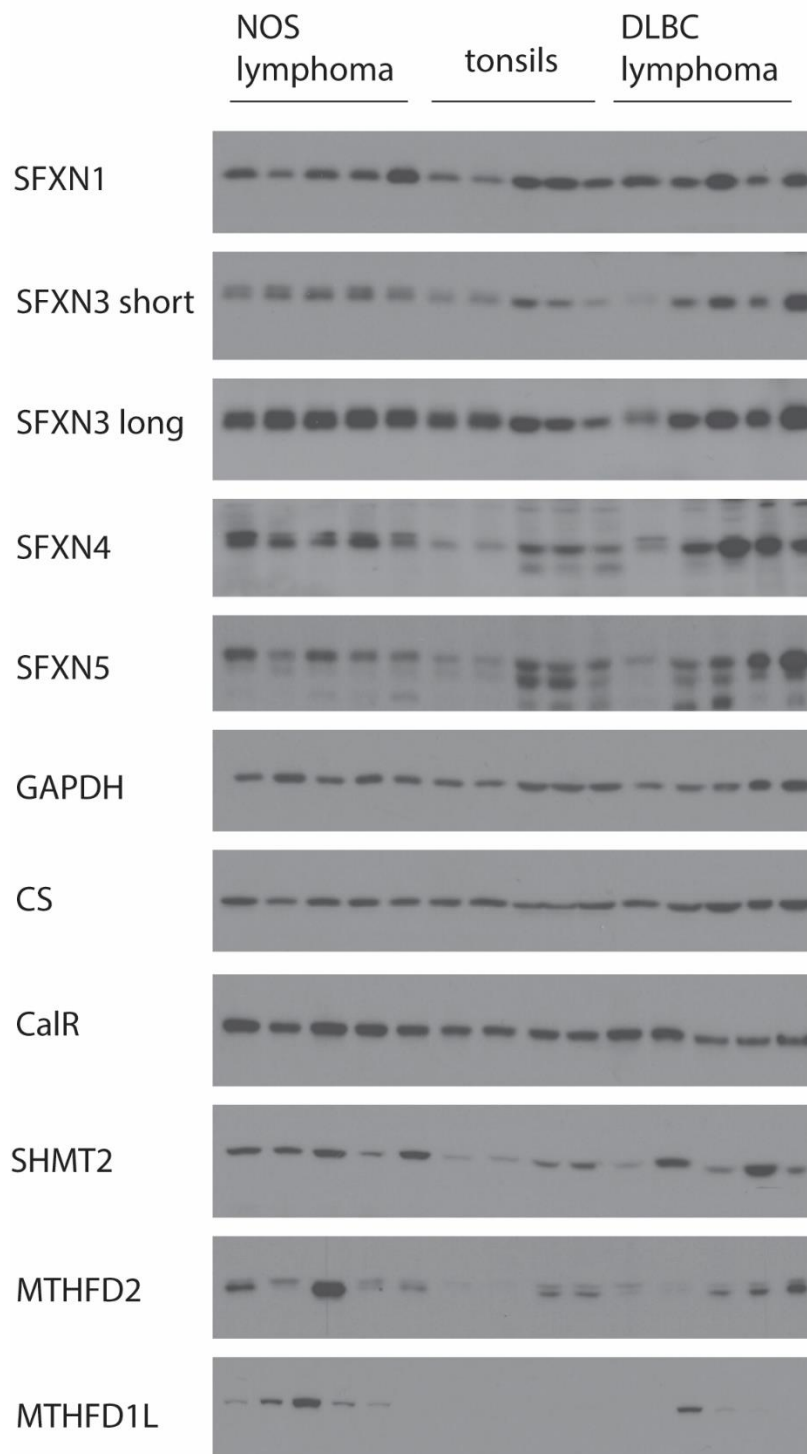


Figure 16: SFXN1 is likely a target of cancer metabolism alterations. SFXN1 is likely overexpressed in human NOS and DLBC lymphoma. CS, GAPDH and CalR are used as loading controls. SHMT2 and MTHFD2 are presented as positive controls. MTHFD1L is likely strictly conserved to cancer samples. Antibodies used SFXN1-5 (Sideroflexin 1-5); GAPDH (Glyceraldehyde 3-phosphate dehydrogenase), CS (citrate synthase), CalR (Calreticulin), SHMT2 (Serine hydroxymethyltransferase 2), MTHFD2 (Methylene-THF dehydrogenases 2), MTHFD1L (Methylene-THF dehydrogenases 1 like). Protein amount was normalized to 50ng per lane.

4 Discussion

Over the past years, serine was highlighted as one of the most important amino acids in one-carbon metabolism. Kory *et al* were recently able to identify that SFXN1 transports cytosolic serine into the mitochondrion. SFXN1 has previously been shown to be important as its loss-of-function causes anemia in mice [55], but the role of SFXN1 remains controversial since later studies identified mutations in a different gene to be responsible for this phenotype [85]. Now that we know its molecular function, which is the transport of serine from the cytosol into the mitochondrion [20], we can study the role of SFXN1 and its homologues *in vivo*.

In our hands SFXN1 is likely to be expressed throughout most organs of the murine system. Tissues such as the liver and the kidney seem to have high expression levels of SFXN1. These findings are consistent with the current literature. SFXN1, as a major player in the one-carbon metabolism, is present in the liver which contributes to many metabolic processes as for example heme synthesis, gluconeogenesis and lipid metabolism [3], [32]. However, tissues such as the heart and skeletal muscle, where SFXN1 should be expressed according to RNA seq data sets, did not show bands for the protein of interest. SFXN3 was identified as a protein specific to the nervous system as before in literature [57], [59]. SFXN5 was shown to have two different isoforms, a long isoform consisting of 340 amino acids, resulting in a size of 37kDa, and a short isoform of 253 amino acids, resulting in a band at 30kDa (NCBI). The RNAseq expression patterns of SFXN2 and SFXN4 did not correlate with the data generated in our hands. To avoid possible bias, it would be important to verify the specificity of the antibodies by using *in vitro* expressed murine SFXN homologues as a control.

The establishment of stable SFXN1 knockout strains was not possible up to this point. A close monitoring of different breedings has revealed that SFXN1 knockout pups die during the first 24 hours. Because of the correct Mendelian inheritance of 1:2:1 (wild type to heterozygous to homozygous) in all born animals [83], we can exclude developmental issues as the cause of mortality. More litters need to be monitored to verify the lethality of SFXN1 loss in the neonatal stage. The presented data is likely correlating with the transient anemia described by Fleming *et al* [55]. Blood smears of newly born animals have to be histologically stained using an iron or Prussian blue staining to verify the presence of sideroblasts [55]. If the anemia phenotype is causing the lethality, alternative solutions are required to help the neonates to overcome the first 24 hours. Firstly, blood of healthy adult mice needs to be collected. The blood cells have to be washed and later on used as an intraperitoneal transfusion for SFXN1 neonates. Transfused blood cells should help the neonates overcome the anemia. Alternatively, we have designed a conditional knockout strategy for SFXN1 based on a floxed allele. By inducing the KO, a tissue specific depletion of SFXN1 will occur.

This may present a feasible substitute to study the effects of SFXN1 loss in adult animals. To maintain the ability to study the global impact of SFXN1 loss inducible knockout animals can be generated using the tamoxifen inducible Cre system.

Due to the lack of SFXN1 KO mice, we moved forward by characterizing SFXN1 Het animals. By losing a copy of SFXN, the serine transport into the mitochondrion is expected to be partially impaired. We expected the amino acid profiling to reveal increased serine and decreased glycine amounts in SFXN1 Het sample when compared to wild type [20]. A trend indicating a rise in serine levels was noted. Amino acids, phenylalanine, tyrosine and proline, involved in ketogenic processes in the liver were significantly decreased in SFXN1 Het samples. In addition, a drop in methionine levels in SFXN1 Het liver samples was detected. Methionine is a major one-carbon source in the liver. Therefore, it would be reasonable that methionine is compensating for the loss of serine-derived one-carbon units resulting in the seen decrease. The loss of sufficient methionine units would explain the decrease in cystathionine indicating alterations in cysteine synthesis and therefore glutathione metabolism, both processes relying on a steady methionine supply [52]. Alternatively, a deficiency in one-carbon units could lead to decreased methionine synthesis.

The liver is involved in the synthesis of purines which are required for cell survival and proliferation [32]. Nucleotide synthesis intermediate aminoimidazole carboxamide ribonucleotide and its nucleoside inosine monophosphate are increased in SFXN1 Het liver samples. The observed alterations lead to the conclusion that the loss of one functional SFXN1 allele is able to induce the accumulation of purine intermediates. Similar trends were already observed in SHMT2-depleted murine livers [86]. An insufficient one-carbon unit supply by the mitochondrial branch of the folate metabolism, alters several metabolic processes due to a limited flux. In addition to the amino acid and purine intermediates, metabolites involved in fatty acid oxidation and urea cycle were altered as well. Phosphoenolpyruvate, a metabolite involved in fatty acid oxidation [8], was diminished in SFXN1 Het livers when compared to wild type. Furthermore, components of the urea cycle such as creatinine, N-acetylglutamate, N-acetylglutamine and ornithine were significantly reduced in our hands. The decrease of ornithine levels and a trend towards an increase of liver arginine levels were expected to occur due to the inhibitory effects of lysine on the urea cycle. Lysine is known to inhibit arginases contributing to the cycle. This inhibitory effect was reported with elevated lysine concentrations in the blood [84]. The lysine accumulation was not significant in our SFXN1 Het plasma samples. A closer examination of lysine metabolism intermediates identified a decrease in up- and downstream targets of this pathway in the livers of SFXN1 het animals. Saccharopine, the precursor molecule of glutamate and α -amino adipate 8-semialdehyde synthesis via lysine degradation, and α -amino adipate, the final product of lysine degradation [87], are both reduced in the SFXN1 Het livers. Lower glutamate levels may be linked to the seen dysregulation of the lysine degradation pathway. However, the exact connection between the pathways is still unclear.

We report that the loss of SFXN 3 has an impact on SFXN1 expression levels in the murine brain. Single cell RNAseq expression patterns have revealed a similar localization of the two homologues. SFXN1 was found in clusters of cerebral cortex astrocytes, neurons, Bergmann glia and oligodendrocyte precursors located in the non-myeloid brain. SFXN3 was located in neurons, pericytes of the brain and endothelial cells. The neuronal localization of the two proteins could be a possible explanation for the observed alterations in SFXN3 KO brains. In contrast, SFXN5 was mainly detected in astrocytes of the cerebral cortex as well as precursor and mature oligodendrocytes. SFXN5 protein levels remained unaffected when comparing SFXN3 and wild type brains. A comparison of kidney and liver tissue, the organs with the highest SFXN1 and low SFXN3 expression (**Figure 6B**), of the same animals did not show a decrease in SFXN1 levels. This alteration in SFXN1 protein levels seems therefore conserved to the brain, in our hands. The presented data shows promising result which need to be verified in future experiments using larger cohorts. Furthermore, a morphological and immunohistological assessment of SFXN3 KO brains needs to be performed.

It would be important to elucidate the mechanism causing the drastic decrease in SFXN1 protein levels in the brains of SFXN3 KO animals. We were not able to connect the loss of SFXN3 to serine transport deficiency. In contrast, significant changes in histidine levels were shown in SFXN3 knockout brains when compared to wild type. As in SFXN3 KO brains, histidine levels were also elevated in SFXN1 Het plasma samples. This amino acid is known to be a limiting factor in THF degradation. Therefore, if SFXN1 or SFXN3 loss are affecting the folate metabolism and therefore promoting the degradation of histidine, THF availability in the cell would increase [88]. The accumulation of proline, which is deaminated in a similar process to histidine [89], would contribute to the hypothesis, that the cells compensate for the impaired flux of one-carbon unites by deaminating other amino acids.

Further investigations are required to reveal the exact localization of SFXN3 in the brain. According to the presented single cell RNA sequencing data sets on SFXN1 and 3 are both located in neurons [82]. The data sets are in accordance with scientific literature presented by Amorim *et al* and Rivell *et al* [57], [59]. However, upon closer examination of the immunoblotting results we discovered that the antibody used by both studies was shown to bind both homologues, SFXN1 and SFXN3. This unspecific binding was already presented by Kory *et al*. In their hands, this antibody also showed an additional binding affinity for SFXN2 [20]. Resulting, brain specific antibodies as well as a SFXN3 specific antibody need to be used to assess the expression of this homologue in the nervous system. The role of serine in brain development revealed its importance in neuronal survival and the maintenance of synaptic plasticity [68]. Due to the high homology between SFXN1 and SFXN3 it is possible that these proteins form a functional complex in the brain to transport serine into the different subtypes of brain cells.

It is hypothesized that SFXN1 and 3 may play a role in diseases connected to the nervous system. Minjarez *et al*/showed in their proteomic-based screen, that SFXN1 is subexpressed in the brains of Alzheimer's patients [90]. Furthermore, Fowler *et al* were able to connect SFXN1 to the neuropathic Charcot-Marie-Tooth disease which is caused by a connexin 32 mutation [91], [92].

The presented data on SFXN1 expression in human lymphoma biopsies may present a possible new target for cancer therapies. Samples of NOS lymphomas as well as two of the DLCL lymphomas show a correlation in SFXN1, SHMT2, MTHFD2 and MTHFD1L overexpression. However, to verify the observed trends, the patient cohort must be increased. The collection of new samples, especially the healthy controls, will require time due to the limited tissue supply. Tonsils used in this study revealed different phenotypes. A likely cause of the observed alterations in the control samples could be linked to a tonsil inflammation. Lymphocytes are activated in a nutrient-dependent manner by cMyc, a transcription factor which is also overexpressed in tumors [52]. Metabolic changes occurring during the activation of lymphocyte proliferation are similar to those occurring in cancer [11], [27]. It would be important to find a more fitting negative control to overcome the observed bias by the overexpression of one-carbon metabolism related proteins. Due to the privacy policy of the Massachusetts General Hospital we were not able to obtain further information on the health state of the donors.

To sum up, SFXN1 was revealed to be the predominantly expressed member of the SFXN family across different tissue types whereas SFXN3 can only be found in the brain. The loss of one functional SFXN1 allele lead in our experiments to alterations of the cellular metabolism. An accumulation of purine synthesis and decrease of urea cycle intermediates were detected in the livers of SFXN1 heterozygous animals resulting from the limited one-carbon flux. We hypothesize that the cell compensates for the insufficient flux of one-carbon units by altering methionine, histidine as well as proline deamination processes. The depletion of SFXN3 lead to a decrease of SFXN1 expression in the adult murine brain. Control tissues such as kidney or liver remain unchanged. We hypothesize that the downregulation of SFXN1 protein levels in SFXN3 KO brains is linked to the localization of the two proteins in neurons. We speculate that both homologous must play a crucial role in neural plasticity by working as functional complexes. A morphological analysis of the SFXN3 KO brains as well as an immunoprecipitation study of SFXN1 and SFXN3 in murine brains could offer valuable insight. The link between neurodegenerative diseases and members of the SFXN family offers additional promising future directions.

The analysis of human cancer samples reveals that SFXN1 is likely upregulated in other not further specified (NOS) and diffuse large B-cell (DLBCL) lymphomas. Over the past years, serine was highlighted as one of the most important amino acids in cancer metabolism. Understanding SFXNs and their functions may also lead to a better understanding of cancer metabolism. Studies were able to identify that activation of serine synthesis and the mitochondrial one-carbon pathway correlates with cancer proliferation and survival [48]. Current strategies for improved cancer treatment focus on the inhibition of folate delivery into the cancer cells [93]. The presented results may indicate novel targets for cancer therapies for both up- (SFXN1) and downstream (MTHFD1L) targets of the one-carbon pathway.

In conclusion, the *in vivo* studies of SFXN1 and SFXN3 mice as well as the initial characterization of lymphomas indicate interesting trends shedding light on the functions of an important but poorly understood family of mitochondrial transporters.

Bibliography

- [1] T. Gabaldón and A. A. Pittis, "Origin and evolution of metabolic sub-cellular compartmentalization in eukaryotes," *Biochimie.*, vol. 119, pp. 262–268, 2015.
- [2] A. Zecchin, P. C. Stapor, J. Goveia, and P. Carmeliet, "Metabolic pathway compartmentalization: an underappreciated opportunity?," *Curr. Opin. Biotechnol.*, vol. 34, pp. 73–81, 2014.
- [3] B. J. Alberts, A. Lewis, and J. Raff, *Molecular biology of the cell*, 6th Editio., no. 574.87 M6/2008. New York: Garland Science, 2015.
- [4] C. M. Metallo and M. G. Vander Heiden, "Understanding Metabolic Regulation and Its Influence on Cell Physiology," *MOLCEL*, vol. 49, no. 3, pp. 388–398, 2013.
- [5] M. Al-habori, "Microcompartmentation, Metabolic Chanelling and Carbon Metabolism," *Int. J. Biochem. Cell Biol.*, vol. 2, no. 94, pp. 123–132, 1995.
- [6] C. M. Agapakis, P. M. Boyle, and P. A. Silver, "Natural strategies for the spatial optimization of metabolism in synthetic biology," *Nat. Chem. Biol.*, vol. 8, no. 6, pp. 527–535, 2012.
- [7] A. Weeks, L. Lund, and F. M. Raushel, "Tunneling of intermediates in enzyme-catalyzed reactions," *Current Opinion in Chemical Biology*, vol. 10, no. 5. pp. 465–472, 2006.
- [8] D. Voet, J. G. Voet, and C. W. Pratt, *Fundamentals of biochemistry life at the molecular level*. 2016.
- [9] A. Wegner, J. Meiser, and D. Weindl, "How metabolites modulate metabolic flux," *Curr. Opin. Biotechnol.*, vol. 34, pp. 16–22, 2015.
- [10] J. S. Andersen and M. Mann, "Organellar proteomics: Turning inventories into insights," *EMBO Reports*, vol. 7, no. 9. pp. 874–879, 2006.
- [11] R. Wang *et al.*, "The Transcription Factor Myc Controls Metabolic Reprogramming upon T Lymphocyte Activation," *Immunity*, 2011.
- [12] H. Vakifahmetoglu-Norberg, A. T. Ouchida, and E. Norberg, "The role of mitochondria in metabolism and cell death," *Biochem. Biophys. Res. Commun.*, vol. 482, no. 3, pp. 426–431, 2017.
- [13] L. Galluzzi *et al.*, "No death without life: Vital functions of apoptotic effectors," *Cell Death and Differentiation*, vol. 15, no. 7. pp. 1113–1123, 2008.
- [14] L. Wiemerslage and D. Lee, "Quantification of mitochondrial morphology in neurites of dopaminergic neurons using multiple parameters.," *J. Neurosci. Methods*, vol. 262, pp. 56–65, Mar. 2016.
- [15] A. I. P. M. De Kroon, D. Dolis, A. Mayer, R. Lill, and B. De Kruijff, "Phospholipid composition of highly purified mitochondrial outer membranes of rat liver and *Neurospora crassa*. Is cardiolipin present in the mitochondrial outer membrane?," *Biochim. Biophys. Acta - Biomembr.*, 1997.

- [16] L. C. Schenkel and M. Bakovic, "Formation and Regulation of Mitochondrial Membranes," *Int. J. Cell Biol.*, vol. 2014, 2013.
- [17] E. Blachly-Dyson and M. Forte, "VDAC channels.," *IUBMB Life*, vol. 52, no. 3–5, pp. 113–118, 2001.
- [18] F. Palmieri and C. L. Pierri, "Mitochondrial metabolite transport," *Essays Biochem.*, vol. 47, pp. 37–52, 2010.
- [19] M. A. Hediger, M. F. Romero, J.-B. Peng, A. Rolfs, H. Takanaga, and E. A. Bruford, "The ABCs of solute carriers: physiological, pathological and therapeutic implications of human membrane transport proteinsIntroduction.," *Pflugers Arch.*, vol. 447, no. 5, pp. 465–468, Feb. 2004.
- [20] N. Kory *et al.*, "SFXN1 is a mitochondrial serine transporter required for one-carbon metabolism," *Science.*, vol. 362, no. 6416, pp. 1–24, Nov. 2018.
- [21] J. M. Berg, J. L. Tymoczko, and L. Stryer, "Glycolysis Is an Energy-Conversion Pathway in Many Organisms," 2002.
- [22] J. Herrmann and J. Riemer, "The Intermembrane Space of Mitochondria," *Antioxid. Redox Signal.*, vol. 13, pp. 1341–1358, 2010.
- [23] J. M. Berg, J. L. Tymoczko, and L. Stryer, "Amino Acids Are Made from Intermediates of the Citric Acid Cycle and Other Major Pathways.," in *Biochemistry.*, 5th editio., New York: W H Freeman, 2002.
- [24] A. S. Ogun and M. Valentine, *Biochemistry, Heme Synthesis*. 2018.
- [25] X. Yuan *et al.*, "Regulation of intracellular heme trafficking revealed by subcellular reporters.," *Proc. Natl. Acad. Sci. U. S. A.*, vol. 113, no. 35, pp. E5144-52, Aug. 2016.
- [26] M. Valko, D. Leibfritz, J. Moncol, M. T. D. Cronin, M. Mazur, and J. Telser, "Free radicals and antioxidants in normal physiological functions and human disease," *International Journal of Biochemistry and Cell Biology*, vol. 39, no. 1. pp. 44–84, 2007.
- [27] M. G. Vander Heiden, L. C. Cantley, and C. B. Thompson, "Understanding the Warburg Effect: The Metabolic Requirements of Cell Proliferation," *Science (80-)*, vol. 324, no. 5930, p. 1029 LP-1033, May 2009.
- [28] K. R. Mattaini, M. R. Sullivan, and M. G. Vander Heiden, "The importance of serine metabolism in cancer," *Journal of Cell Biology*, vol. 214, no. 3. pp. 249–257, 2016.
- [29] S. J. Duthie, "Folic acid deficiency and cancer: mechanisms of DNA instability.," *Br. Med. Bull.*, vol. 55, no. 3, pp. 578–592, 1999.
- [30] R. J. Cook, "Defining the steps of the folate one-carbon shuffle and homocysteine metabolism," *American Journal of Clinical Nutrition*, 2000.
- [31] P. Vallance, "Homocysteine in Health and Disease.," *Journal of the Royal Society of Medicine*, vol. 95, no. 3. p. 159, Mar-2002.
- [32] G. S. Ducker and J. D. Rabinowitz, "One-Carbon Metabolism in Health and Disease," *Cell Metab.*, vol. 25, no. 1, pp. 27–42, 2017.

- [33] Y. Zheng and L. C. Cantley, "Toward a better understanding of folate metabolism in health and disease," *J. Exp. Med.*, vol. 216, no. 2, pp. 253–266, 2018.
- [34] M. Visentin, R. Zhao, and I. D. Goldman, "Augmentation of Reduced Folate Carrier-Mediated Folate / Antifolate Transport through an Antiport Mechanism with 5-Aminoimidazole-4-Carboxamide Riboside Monophosphate," *Mol Pharmacol*, vol. 82, no. 2, pp. 209–216, 2012.
- [35] R. Zhao, N. Diop-Bove, M. Visentin, and I. D. Goldman, "Mechanisms of Membrane Transport of Folates into Cells and Across Epithelia," *Annu. Rev. Nutr.*, vol. 31, no. 1, pp. 177–201, 2011.
- [36] A. S. Tibbetts and D. R. Appling, "Compartmentalization of Mammalian Folate-Mediated One-Carbon Metabolism," 2010.
- [37] C. A. Lewis *et al.*, "Tracing Compartmentalized NADPH Metabolism in the Cytosol and Mitochondria of Mammalian Cells," *Mol. Cell*, 2014.
- [38] G. S. Ducker *et al.*, "Reversal of Cytosolic One-Carbon Flux Compensates for Loss of the Mitochondrial Folate Pathway Article Reversal of Cytosolic One-Carbon Flux Compensates for Loss of the Mitochondrial Folate Pathway," *Cell Metab.*, vol. 23, no. 6, pp. 1140–1153, 2016.
- [39] E. J. Tucker *et al.*, "Mutations in MTFMT underlie a human disorder of formylation causing impaired mitochondrial translation.," *Cell Metab.*, vol. 14, no. 3, pp. 428–434, Sep. 2011.
- [40] D. R. Minton *et al.*, "Serine Catabolism by SHMT2 Is Required for Proper Mitochondrial Translation Initiation and Maintenance of Formylmethionyl-tRNAs," *Mol. Cell*, 2018.
- [41] B. Chaneton *et al.*, "Serine is a natural ligand and allosteric activator of pyruvate kinase M2," *Nature*, vol. 491, p. 458, Oct. 2012.
- [42] W. Pfendner and L. I. Pizer, "The metabolism of serine and glycine in mutant lines of Chinese hamster ovary cells.," *Arch. Biochem. Biophys.*, vol. 200, no. 2, pp. 503–512, Apr. 1980.
- [43] A. W. El-Hattab, "Serine biosynthesis and transport defects," *Mol. Genet. Metab.*, 2016.
- [44] L. Galluzzi *et al.*, "Autophagy in malignant transformation and cancer progression.," *EMBO J.*, vol. 34, no. 7, pp. 856–880, Apr. 2015.
- [45] A. C. Newman and O. D. K. Maddocks, "Serine and Functional Metabolites in Cancer," *Trends Cell Biol.*, vol. xx, pp. 1–13, 2017.
- [46] J. Meiser and A. Vazquez, "Give it or take it: the flux of one-carbon in cancer cells," *FEBS Journal*, vol. 283, no. 20, pp. 3695–3704, 2016.
- [47] M. Pietzke, J. Meiser, and A. Vazquez, "Formate metabolism in health and disease," *Mol. Metab.*, 2019.
- [48] J. W. Locasale, "Serine, glycine and the one-carbon cycle: cancer metabolism in full circle," *Nat Rev Cancer*, vol. 13, no. 8, pp. 572–583, 2013.

- [49] A. Carrer and K. E. Wellen, "Metabolism and epigenetics : a link cancer cells exploit," *Curr. Opin. Biotechnol.*, vol. 34, pp. 23–29, 2015.
- [50] I. Amelio, F. Cutruzzola, A. Antonov, M. Agostini, and G. Melino, "Serine and glycine metabolism in cancer," *Trends Biochem. Sci.*, vol. 39, no. 4, pp. 191–198, 2014.
- [51] S. Lucas, G. Chen, S. Aras, and J. Wang, "Serine catabolism is essential to maintain mitochondrial respiration in mammalian cells," *Life Sci. Alliance*, vol. 1, no. 2, pp. 1–10, 2018.
- [52] M. Yang and K. H. Vousden, "Serine and one-carbon metabolism in cancer," *Nat. Publ. Gr.*, 2016.
- [53] M. D. Fleming, "Congenital Sideroblastic Anemias : Iron and Heme Lost in Mitochondrial Translation," *Blood*, pp. 525–531, 2011.
- [54] X. Li *et al.*, "Developmental Expression of sideroflexin Family Genes in Xenopus Embryos," *Dev. Dyn.*, no. August, pp. 2742–2747, 2010.
- [55] M. D. Fleming, D. R. Campagna, J. N. Haslett, C. C. Trenor, and N. C. Andrews, "A mutation in a mitochondrial transmembrane protein is responsible for the pleiotropic hematological and skeletal phenotype of flexed-tail (f/f) mice," *Genes Dev.*, vol. 15, no. 6, pp. 652–657, 2001.
- [56] D. J. Pagliarini *et al.*, "A Mitochondrial Protein Compendium Elucidates Complex I Disease Biology," *Cell*, 2008.
- [57] A. Rivell, R. S. Petralia, Y. X. Wang, M. P. Mattson, and P. J. Yao, "Sideroflexin 3 is a Mitochondrial Protein Enriched in Neurons," *NeuroMolecular Med.*, no. 0123456789, 2019.
- [58] F. Simunovic *et al.*, "Gene expression profiling of substantia nigra dopamine neurons: further insights into Parkinson's disease pathology," *Brain*, 2009.
- [59] I. S. Amorim *et al.*, "Sideroflexin 3 is an α -synuclein-dependent mitochondrial protein that regulates synaptic morphology," *J. Cell Sci.*, vol. 130, no. 2, pp. 325–331, 2017.
- [60] G. J. Hildick-Smith *et al.*, "Macrocytic Anemia and Mitochondriopathy Resulting from a Defect in Sideroflexin 4," *Am. J. Hum. Genet.*, vol. 93, no. 5, pp. 906–914, 2013.
- [61] K. Sofou *et al.*, "Prenatal onset of mitochondrial disease is associated with sideroflexin 4 deficiency," *Mitochondrion*, vol. 47, no. May, pp. 76–81, 2019.
- [62] S. I. Miyake, T. Yamashita, M. Taniguchi, M. Tamatani, K. Sato, and M. Tohyama, "Identification and characterization of a novel mitochondrial tricarboxylate carrier," *Biochem. Biophys. Res. Commun.*, vol. 295, no. 2, pp. 463–468, 2002.
- [63] E. E. Mon, F. Y. Wei, R. N. R. Ahmad, T. Yamamoto, T. Moroishi, and K. Tomizawa, "Regulation of mitochondrial iron homeostasis by sideroflexin 2," *J. Physiol. Sci.*, vol. 69, no. 2, pp. 359–373, 2019.
- [64] Z. Long, H. Li, Y. Du, and B. Han, "Congenital sideroblastic anemia : Advances in gene mutations and pathophysiology," *Gene*, vol. 668, no. April, pp. 182–189, 2018.

- [65] A. E. Beaudin and P. J. Stover, "Insights into metabolic mechanisms underlying folate-responsive neural tube defects: A minireview," *Birth Defects Research Part A - Clinical and Molecular Teratology*. 2009.
- [66] A. J. MacFarlane *et al.*, "Mthfd1 is an essential gene in mice and alters biomarkers of impaired one-carbon metabolism," *J. Biol. Chem.*, 2009.
- [67] J. Momb *et al.*, "Deletion of Mthfd1l causes embryonic lethality and neural tube and craniofacial defects in mice," *Proc. Natl. Acad. Sci. U. S. A.*, 2013.
- [68] S. Furuya and M. Watanabe, "Novel neuroglial and gliogial relationships mediated by L-serine metabolism.," *Arch. Histol. Cytol.*, vol. 66, pp. 109–121, 2003.
- [69] J. Nikkanen *et al.*, "Mitochondrial DNA Replication Defects Disturb Cellular dNTP Pools and Remodel One-Carbon Metabolism," *Cell Metab.*, vol. 23, no. 4, pp. 635–648, 2016.
- [70] L. Sun *et al.*, "cMyc-mediated activation of serine biosynthesis pathway is critical for cancer progression under nutrient deprivation conditions," *Nat. Publ. Gr.*, vol. 25, no. 4, pp. 429–444, 2015.
- [71] A. Vazquez, E. K. Markert, and Z. N. Oltvai, "Serine biosynthesis with one carbon catabolism and the glycine cleavage system represents a novel pathway for ATP generation," *PLoS One*, vol. 6, no. 11, pp. 1–10, 2011.
- [72] M. Laanpere, S. Altmäe, A. Stavreus-Evers, T. K. Nilsson, A. Yngve, and A. Salumets, "Folate-mediated one-carbon metabolism and its effect on female fertility and pregnancy viability," *Nutrition Reviews*, vol. 68, no. 2. pp. 99–113, 2010.
- [73] NCI, "National Cancer Institute - Lymphoma," 2019. [Online]. Available: <https://www.cancer.gov/types/lymphoma>.
- [74] E. N. Mugnaini and N. Ghosh, "Lymphoma.," *Prim. Care*, vol. 43, no. 4, pp. 661–675, Dec. 2016.
- [75] E. S. Jaffe, "Diagnosis and classification of lymphoma: Impact of technical advances," *Semin. Hematol.*, vol. 56, no. 1, pp. 30–36, 2019.
- [76] D. Fuchs, "Diffuse large B-cell lymphoma," *Memo - Magazine of European Medical Oncology*. 2019.
- [77] R. Küppers, "Mechanisms of B-cell lymphoma pathogenesis," *Nature Reviews Cancer*. 2005.
- [78] H. Yang, H. Wang, and R. Jaenisch, "Generating genetically modified mice using CRISPR/Cas-mediated genome engineering," *Nat. Protoc.*, 2014.
- [79] K. Birsoy, T. Wang, W. W. Chen, E. Freinkman, M. Abu-Remaileh, and D. M. Sabatini, "An Essential Role of the Mitochondrial Electron Transport Chain in Cell Proliferation Is to Enable Aspartate Synthesis," *Cell*, 2015.
- [80] W. W. Chen, E. Freinkman, T. Wang, K. Birsoy, and D. M. Sabatini, "Absolute Quantification of Matrix Metabolites Reveals the Dynamics of Mitochondrial Metabolism," *Cell*, vol. 166, no. 5, p. 1324–1337.e11, 2016.

- [81] I. Papatheodorou *et al.*, “Expression Atlas: Gene and protein expression across multiple studies and organisms,” *Nucleic Acids Res.*, 2018.
- [82] N. Schaum *et al.*, “Single-cell transcriptomics of 20 mouse organs creates a Tabula Muris,” *Nature*, 2018.
- [83] T. Harel, D. Pehlivan, C. T. Caskey, and J. R. Lupski, “Mendelian, Non-Mendelian, Multigenic Inheritance, and Epigenetics,” in *Rosenberg’s Molecular and Genetic Basis of Neurological and Psychiatric Disease: Fifth Edition*, 2014.
- [84] M. Statter, A. Russell, and S. Rotaro, “Competitive interrelationships between lysine and arginine in rat liver under normal conditions and in experimental hyperammonemia,” *Life Sci.*, vol. 22, no. 5, pp. 2097–2101, 1978.
- [85] D. R. Richardson *et al.*, “Mitochondrial iron trafficking and the integration of iron metabolism between the mitochondrion and cytosol,” *Proceedings of the National Academy of Sciences of the United States of America*, vol. 107, no. 24, pp. 10775–10782, 2010.
- [86] H. Tani *et al.*, “Disruption of the mouse *Shmt2* gene confers embryonic anaemia via foetal liver-specific metabolomic disorders,” *Sci. Rep.*, 2019.
- [87] F. C. I. Fellows and M. H. R. Lewis, “Lysine metabolism in mammals,” *Biochem. J.*, 1973.
- [88] N. Kanarek *et al.*, “Histidine catabolism is a major determinant of methotrexate sensitivity,” *Nature*. 2018.
- [89] K. Vivekanandan, “Oxidative decarboxylation and deamination of proline, histidine, arginine, lysine and tyrosine by N-chloronicotinamide in aqueous acetic acid medium. A kinetic study,” *Oxid. Commun.*, 2004.
- [90] B. Minjarez *et al.*, “Identification of proteins that are differentially expressed in brains with Alzheimer’s disease using iTRAQ labeling and tandem mass spectrometry,” *J. Proteomics*, 2016.
- [91] S. L. Fowler, M. Akins, H. Zhou, D. Figeys, and S. A. L. Bennett, “The liver connexin32 interactome is a novel plasma membrane-mitochondrial signaling nexus,” *J. Proteome Res.*, 2013.
- [92] J. Bergoffen *et al.*, “Connexin mutations in X-linked Charcot-Marie-Tooth disease,” *Science (80-.)*, 1993.
- [93] A. K. Fotoohi and F. Albertioni, “Mechanisms of antifolate resistance and methotrexate efficacy in leukemia cells,” *Leukemia and Lymphoma*, vol. 49, no. 3, pp. 410–426, 2008.

List of Figures

- Figure 1: Mitochondria are compartmentalized organelles in eukaryotes.** Indicated are schematic depictions of the two limiting membranes (outer and inner) as well as the intermembrane space and the mitochondrial matrix. 8
- Figure 2: One-carbon metabolism is compartmentalized into a cytosolic and a mitochondrial branch.** A: Folates are transported via solute carrier 19A1 and 46A1 into the cytosol. B: Cytosolic branch of the one-carbon metabolism. Enzymes in the cytosol contribute towards purine and methionine synthesis through one-carbon and formate units from the mitochondrial branch. C: Mitochondrial branch fuels the glycine and formate synthesis. Small molecules can enter the inner mitochondrial membrane through three different transporters; serine via Sideroflexin 1, glycine via SLC25A38 and formate via an unknown transporter. The figure was adapted from Zheng *et al* [33]. 12
- Figure 3: Serine pools are replenished through different pathways.** A: Serine *de novo* synthesis. B: Catabolic processes retrieving serine from autophagy, phospholipid metabolism and diet. C: Serine is made via the one-carbon metabolism. 14
- Figure 4: SFXN1 is a transmembrane protein located in mitochondria and expressed across eukaryotic organisms.** A: Schematic depiction of SFXN1. SFXN1 has five transmembrane domains (matrix: mitochondrial matrix; IMS: intermembrane space). The figure was adapted from Kory *et al* [20]. B: Homology alignment of the five different SFXNs using ClustalW (Hs: *Homo sapiens*, Mm: *Mus musculus*, Dr: *Danio rerio*, Gg: *Gallus gallus*, Xl: *Xenopus laevis*). Adapted from Li *et al* [54] 16
- Figure 5: SFXN1 is likely the predominantly expressed isoform in human tissue samples.** A: Generated heatmap of the SFXN1-5 expression levels in different adult human tissues such as, brain, spinal cord, heart, lung, kidney, pancreas, spleen, ovaries and testis. Expression levels were quantified as TPM (transcripts per minute). The heatmap was generated using the FANTOM5 RNA seq data set (range: 0-41 TPM). B: Heatmap of SFXN1-5 transcription levels in the human cerebral cortex, cerebellum, lung, liver, adrenal gland, pancreas, spleen, reproductive organs and skeletal muscle. The heatmap was generated using the GTEx RNA seq data set (range: 0-161 TPM). C: Protein expression levels of human SFXN1-5 in cerebral cortex, spinal cord, heart, lung, liver, kidney, adrenal gland, pancreas and the reproductive organs. 32
- Figure 6: Global SFXN expression in the murine system reveals SFXN1 as the predominantly expressed homologue.** A: Generated heatmap of the SFXN1-5 expression levels in different adult murine tissues. Expression levels were quantified as TPM (transcripts per minute). The heatmap was made using the FANTOM5 RNA seq data set (range: 0-220 TPM). B: SFXN1-5 expression across different murine tissues. Antibodies used SFXN1-5 (Sideroflexin 1-5); GAPDH (Glyceraldehyde 3-phosphate dehydrogenase), CS (citrate synthase), CalR (Calreticulin). Protein amount was normalized to 40ng per lane. # = sample used from another animal; * = unspecific bands 34

Figure 7: Genotyping reveals a successful heterozygous deletion of SFXN1. A: Primer pairs designed to flank the cutting site of the SFXN1 sgRNA used for the creation of the KO (green: NGS sequencing primers; purple: Conventional genotyping primers). B: Next Generation Sequencing results are aligned with a NCBI genomic sequence of SFXN1. The genotyping results reveal an 8 base pair deletion in SFXN1. The alignment was made using the SnapGene Software. C: Representative PCR genotyping gel of a SFXN1 litter. Genotyping was verified using Transnetyx. A positive control for the wild type allele is indicated (CTRL WT). A positive control for the knockout was a first-generation tail sample missing 2 base pairs (CTRL KO). NTC indicates the negative control.35

Figure 8: Genotyping reveals a successful deletion in SFXN3. A: Primer pairs designed to flank the cutting site of the SFXN3 sgRNA used for the creation of the KO (green: NGS sequencing primers; purple: Conventional genotyping primers). B: Next Generation Sequencing results are aligned with a NCBI genomic sequence of SFXN3. The genotyping results reveal a 29 and 35 base pair deletion in SFXN3. The alignment was made using the SnapGene Software. C: Representative PCR genotyping gel of SFXN3 animals. A positive control for the wild type allele is indicated (CTRL WT). NGS verified mice were used as controls for the knockouts (SFXN3 29KO, SFXN3 35KO, SFXN3 29/35KO) and heterozygotes (SFXN3 29Het, SFXN3 35Het). NTC indicates the negative control.36

Figure 9: Basic characterization of SFXN1 and 3 mice. A: Distribution of genotypes in weaned adult mice. A lack of SFXN1 KO animals is to be noted (mean \pm SD; n of SFXN1 Het x Het litters=14; n of SFXN3 Het x Het litters=8; Two-tailed Mann-Whitney test; p-value=0.05; ***p \leq 0.0002). B: Ratio of SFXN1 neonates from heterozygous breedings surviving until adulthood (mean \pm SD; n of litters=7; Unpaired two-tailed t test with Welch's correction; p-value=0.05). C: Ratio of SFXN3 neonates surviving until adulthood (mean \pm SD; n of litters=9; Unpaired two-tailed t test with Welch's correction; p-value=0.05). All breeding schemes were included. D: Measurements of blood glucose levels in male animals after 18 hours of fasting (mean \pm SD; n=4; ordinary one-way ANOVA with Tukey's multiple comparisons test; p-value=0.05). E: Body mass difference of male animals 26 hours before and after an 18 hour fasting period (mean \pm SD; n=4; Kruskal-Wallis with Dunn's multiple comparisons test; p-value=0.05). F: Body mass of male SFXN1 Het, SFXN3 29KO and wild type animals over the course of six weeks (mean \pm SD; n=5 per genotype). G: Body mass of female SFXN1 Het, SFXN3 29KO and wild type animals over the course of six weeks (mean \pm SD; n=5 per genotype).38

Figure 10: Characterization of SFXN1 heterozygous breeding litters. A: Representative images of SFXN1 litters on the day of birth. Paler animals are indicated by the yellow arrow. B: Genotyping gel of a complete SFXN1 litter including pups which were found dead and their litter mates. Deletions were verified by Transnetyx. C: Distribution of the genotypes detected in six consecutive litters revealing the expected Mendelian inheritance of a heterozygous breeding (mean \pm SD).39

Figure 11: The loss of a functional SFXN1 allele reveals a decrease in SFXN1 protein levels. A: A loss of a functional SFXN1 copy accounts for 50% of protein levels in tissues

of age-matched female animals. Antibodies used SFXN1-5 (Sideroflexin 1-5); GAPDH (Glyceraldehyde 3-phosphate dehydrogenase), CS (citrate synthase), CalR (Calreticulin). B: The 50% loss of protein levels in SFXN1 Het livers is replicable. Age-matched SFXN1 Het wildtype animals were used (n=4 per genotype). Antibodies used SFXN1, 5 (Sideroflexin 1 and 5); GAPDH (Glyceraldehyde 3-phosphate dehydrogenase), CS (citrate synthase), CalR (Calreticulin). Protein amount was normalized to 40ng per lane for both experiments. * = unspecific bands41

Figure 12: The loss of a functional SFXN1 allele leads to alterations of the murine metabolism. A: Metabolic profiling of amino acids in SFXN1 Het liver samples (mean \pm SD; n=4 per genotype; Unpaired two-tailed t-tests with Welch's correction or Mann-Whitney test; *:p \leq 0.05, **:p \leq 0.001). B: Metabolic profiling of TCA cycle related metabolites in SFXN1 Het liver samples (mean \pm SD; n=4 per genotype; Unpaired two-tailed t-tests with Welch's correction or Mann-Whitney test; **:p \leq 0.001). C: Metabolic profiling of purine synthesis intermediates in SFXN1 Het liver samples (mean \pm SD; n=4 per genotype; Unpaired two-tailed t-tests with Welch's correction or Mann-Whitney test; *:p \leq 0.05, **:p \leq 0.001). D: Metabolic profiling of mitochondrial metabolism related molecules in SFXN1 Het liver samples (mean \pm SD; n=4 per genotype; Unpaired two-tailed t-tests with Welch's correction or Mann-Whitney test; *:p \leq 0.05, ***:p \leq 0.0001). E: Metabolic profiling of lysine metabolism intermediates in SFXN1 Het liver samples (mean \pm SD; n=4 per genotype; Unpaired two-tailed t-tests with Welch's correction or Mann-Whitney test; **:p \leq 0.001).....43

Figure 13: Loss of SFXN3 alters SFXN1 expression in the murine brain. A: SFXN1 expression in SFXN3 knockout brains. SFXN1 levels alter when compared to wild type samples. Antibodies used SFXN1, 4, 5 (Sideroflexin 1, 4, 5); GAPDH (Glyceraldehyde 3-phosphate dehydrogenase), CS (citrate synthase), CalR (Calreticulin), SHMT2 (Serine hydroxymethyltransferase 2). Protein amount was normalized to 40ng per lane. B: Signal quantification of SFXN1 bands. Bands were normalized to GAPDH and the fold change was calculated by normalizing to wild type (mean \pm SD; n=2; Two-way ANOVA with Dunnett's multiple comparisons; *:p \leq 0.05; ***:p \leq 0.0001). C: t-SNE cluster of single-cell RNA expression data of SFXN1 in the non-myeloid brain (*Tabula Muris*). D: t-SNE cluster of single-cell RNA expression data of SFXN3 in the non-myeloid brain (*Tabula Muris*). E: t-SNE cluster of single-cell RNA expression data of SFXN5 in the non-myeloid brain (*Tabula Muris*).44

Figure 14: The loss of SFXN3 does not alter serine and glycine levels in the murine brain. A: Metabolic profiling of one-carbon metabolism related intermediates in SFXN3 knockout brain samples (mean \pm SD; n=4 per genotype; Kruskal-Wallis with Dunn's multiple comparisons test; p-value=0.05). B: Metabolic profiling of TCA cycle intermediates in SFXN3 knockout brain samples. (mean \pm SD; n=4 per genotype; ordinary one-way ANOVA with Tukey's multiple comparisons test or Kruskal-Wallis with Dunn's multiple comparisons test; p-value=0.05). C: Metabolic profiling of amino acids in SFXN3 knockout brain samples. (mean \pm SD; n=4 per genotype; ordinary one-way ANOVA with Tukey's multiple

comparisons test or Kruskal-Wallis with Dunn's multiple comparisons test; *:p≤0.05, **:p≤0.001).....45

Figure 15: The changes in SFXN1 expression levels of SFXN3 KO mice are specific to the brain. A: The expression of SFXN1 in SFXN3 KO murine kidney and liver tissues remains at wild type levels. Antibodies used SFXN1 (Sideroflexin 1); GAPDH (Glyceraldehyde 3-phosphate dehydrogenase), CS (citrate synthase), CalR (Calreticulin), SHMT2 (Serine hydroxymethyltransferase 2). Protein amount was normalized to 40ng per lane. * = unspecific bands B: Metabolic profiling of TCA cycle intermediates in SFXN3 KO kidney samples. (mean ± SD; n=4 per genotype; ordinary one-way ANOVA with Tukey's multiple comparisons test or Kruskal-Wallis with Dunn's multiple comparisons test; p=0.05). C: Metabolic profiling of amino acids in SFXN3 KO kidney samples. (mean ± SD; n=4 per genotype; ordinary one-way ANOVA with Tukey's multiple comparisons test or Kruskal-Wallis with Dunn's multiple comparisons test; p=0.05).47

Figure 16: SFXN1 is likely a target of cancer metabolism alterations. SFXN1 is likely overexpressed in human NOS and DLCL lymphoma. CS, GAPDH and CalR are used as loading controls. SHMT2 and MTHFD2 are presented as positive controls. MTHFD1L is likely strictly conserved to cancer samples. Antibodies used SFXN1-5 (Sideroflexin 1-5); GAPDH (Glyceraldehyde 3-phosphate dehydrogenase), CS (citrate synthase), CalR (Calreticulin), SHMT2 (Serine hydroxymethyltransferase 2), MTHFD2 (Methylene-THF dehydrogenases 2), MTHFD1L (Methylene-THF dehydrogenases 1 like). Protein amount was normalized to 50ng per lane.49

List of Tables

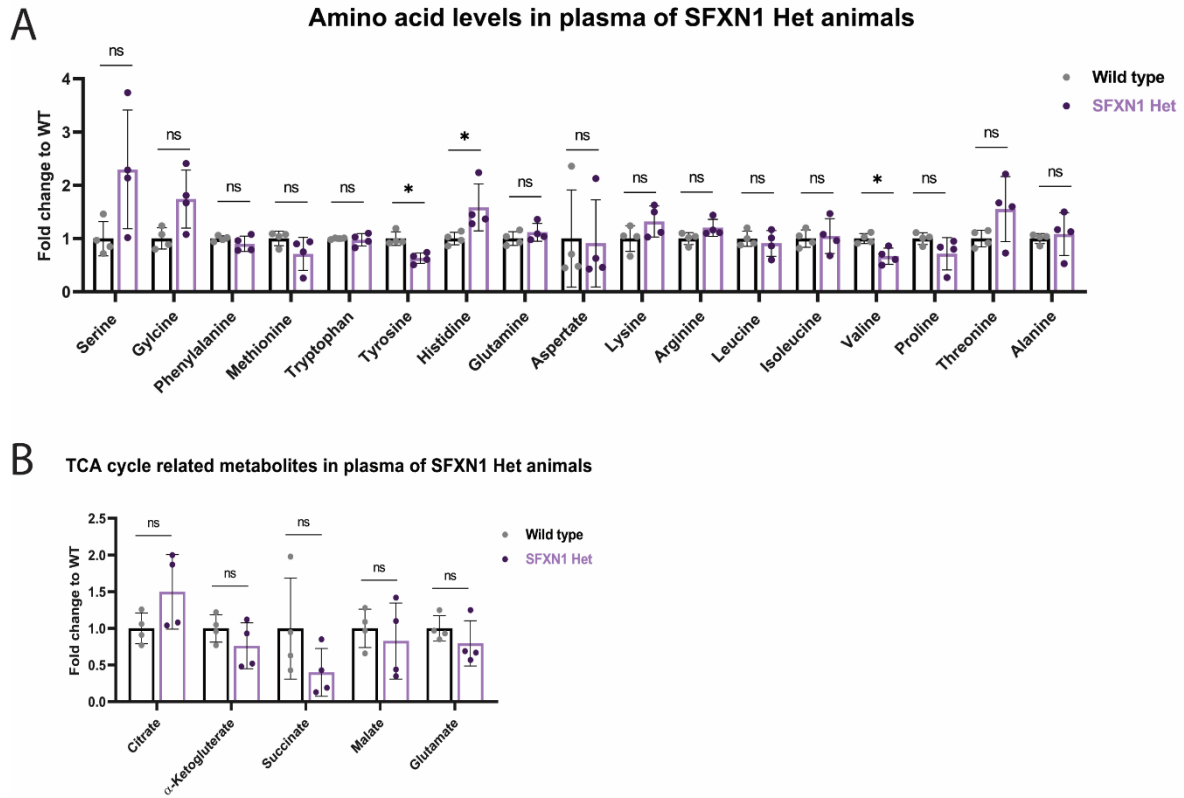
Table 1: Small guide RNAs designed to target SFXN1 and SFXN3	22
Table 2: Sequences of PCR primers made for both genotyping approaches.....	24
Table 3: Temperature Profile for both NGS Sequencing PCRs.....	24
Table 4: Temperature Profile for the SFXN1 genotyping PCR	25
Table 5: Temperature Profile for the SFXN3 genotyping PCR	25
Table 6: Primary antibodies used in murine and human samples.....	28

List of Abbreviations

ATP	Adenosine Triphosphate
OMM	Outer Mitochondrial Membrane
IMM	Inner Mitochondrial Membrane
OXPHOS	Oxphos
SFXNs	Sideroflexins
TCA	Tricarboxylic Acid
NADH	Nicotinamide Adenine Dinucleotide
FADH2	Flavin Adenine Dinucleotide Hydroquinone
ROS	Reactive Oxygen Species
DHF	Dihydrofolate
THF	Tetrahydrofolate
DHFR	Dihydrofolate Reductase
SHMT1	Serine Hydroxymethyltransferase 1
dTMP	Deoxythymidine Monophosphate
TYMS	Thymidylate Synthase
MTHFR	Methylene Tetrahydrofolate Reductase
MTHFD1	5,10-Methylene-THF Dehydrogenase 1
SHMT2	Serine Hydroxymethyltransferase 2
MTHFD2L	Methylene-THF Dehydrogenases Like 1
MTHFD1L	Methylene-THF Dehydrogenases Like 2
MTFHMT	Methionyl-tRNA Formyltransferase
fMet-tRNAs	Formylated Initiator Methionine-Trnas
PHGDH	Phosphoglycerate Dehydrogenase
PSAT	Phosphoserine Aminotransferase
PSP	Phosphoserine Phosphatase
SAM	S-Adenosylmethionine
SFXN1	Sideroflexin 1
SFXN2	Sideroflexin 2
SFXN3	Sideroflexin 3
SFXN4	Sideroflexin 4
SFXN5	Sideroflexin 5
AICAR	Aminoimidazole Carboxamide Ribonucleotide
GAR	Glycinamide Ribonucleotide
CSA	Congenital Sideroblastic Anemia
HL	Hodgkin Lymphoma
NHL	Non-Hodgkin Lymphomas
CLL	Chronic Lymphocytic Leukemia
MCL	Mantle Cell Lymphoma
DLBCL	Diffuse Large B-Cell Lymphoma

NOS L	Not Further Specified Lymphoma
NCI	National Cancer Institute
KO	Knockout
CRISPR	Clustered Regularly Interspaced Short Palindromic Repeats
GEM	Genetically Engineered Models
sgRNAs	Small Guide RNAs
PMSG	Pregnant Mare Serum Gonadotropin
hCG	Human Chorionic Gonadotropin
KSOM	Potassium Simplex Optimization Medium
PCR	Polymerase Chain Reaction
BCA	Bicinchoninic Acid
SDS PAGE	Sodium Dodecyl Sulfate Polyacrylamide Gel Electrophoresis
TBS	Tris Buffered Saline
TBS-T	Tris Buffered Saline with Tween
GAPDH	Glyceraldehyde 3-Phosphate Dehydrogenase
CS	Citrate Synthase
CaR	Calreticulin
LC/MS	Liquid Chromatography-Mass Spectrometry
EDTA	Ethylenediaminetetraacetic Acid
RNAseq	RNA sequencing
TPM	Transcripts per Minute
SFXN1 Het	Heterozygous SFXN1
WT	Wild Type
SFXN3 KO	Homozygous SFXN3 Knockout
CTRL	Control
NTC	Non Template Control

Supplementary Figure 1:



Supplementary Figure 1: Metabolic profiling of SFXN1 Het plasma samples reveals changes in amino acid levels. A: Metabolic profiling of amino acids in SFXN1 Het plasma samples (mean \pm SD; n=4 per genotype; Unpaired two-tailed t-tests with Welch's correction or Mann-Whitney test; *:p \leq 0.05,). B: Metabolic profiling of TCA cycle related metabolites in SFXN1 Het plasma samples (mean \pm SD; n=4 per genotype; Unpaired two-tailed t-tests with Welch's correction or Mann-Whitney test; p=0.05).